

**Federal Ministry of Education  
and Research (BMBF), Germany**

**Ministry of Science, Technology  
and Space (MOST), Israel**

**Joint German-Israeli Water Technology Research Program**

**JOINT FINAL REPORT**

**For the Period: 01/07/2021**

**until 01/07/2024**

German Project Number: 02WIL1605

Israeli Project Number: WT2003

Title of German Project: CO<sub>2</sub> reduction in the oxidation of micropollutants - energy intensive  
vs. novel solar-based processes.

Title of Israeli Project:

הפחתה של CO<sub>2</sub> בחמצון מיקרו מזהמים – תהליכים עתירי אנרגיה לעומת תהליכים חדשניים  
מבוססי קרינה סולרית.

Israeli Principal Investigator -- including Institution and Department:

Prof. Hadas Mamane

Tel Aviv University, Faculty of Engineering

Environmental Engineering program, school of Mechanical Engineering,

German Principal Investigator -- including Institution and Department:

Eng. Christiane Chaumette

Fraunhofer Institute for Interfacial Engineering and Biotechnology IGB

Department of Innovation Field Water

Signatures of

**Israeli** Principal Investigator(s):

Date: 08.10.2024

Prof. Hadas Mamane

**German** Principal Investigator(s):

Date: 08.10.2024

Eng. Christiane Chaumette

Christiane  
Chaumette

Digital unterschrieben  
von Christiane  
Chaumette  
Datum: 2024.10.08  
18:47:55 +02'00'

### Original Milestones

<b>Milestone (MS) Number</b>	<b>Milestone Name</b>	<b>Work package (WP)</b>	<b>Progress During the Last Year</b>	<b>Due vs. completion date.</b>	<b>Was the MS achieved per the original plan?</b>	<b>Reason for Changes and/or delays in MS</b>
<b>M1 Fraunhofer</b>	Data collection defined	WP1 Definition of treatment efficiency. Data review on various Advanced Oxidation Processes (AOPs).	Accomplished Reported in 2022.	Accomplished in September 2021 according to schedule	Yes	
<b>M2 TAU</b>	Catalyst system determined and light integration defined	WP2 Catalyst production. Membrane coating. LED integration for Test System 1 (1 L/h).	Accomplished Reported in 2022.	Accomplished in January 2022 according to schedule	Yes	
<b>M3 Fraunhofer</b>	Pollutant degradation and process parameters quantified	WP3 Testing of Test System 1 with spiked effluent from the Stuttgart Bösau wastewater treatment plant.	Accomplished Reported in 2023.	Accomplished in August 2022 by 2 month delay.	Yes in delay	Dealy in reactor shipping to Germany due to shipment company.
<b>M4 TAU</b>	Performance in long-term demonstration quantified	WP4 Testing of Test System 1 with spiked water streams or effluent	Accomplished Reported in 2022.	July 2022	Yes	

		after ultrafiltration (UF) from the Shafdan plant.				
		WP5 Catalyst production. Membrane coating. LED integration for Test System 2 (10 L/h).	Accomplished	Due date: October 2022, accomplished by September 23.	Yes in delay	The design was complex and took longer than expected. The manufacturing process was also delayed and faced a chain of design, technical and thermal issues that had to be addressed before operating.
		WP6 Long-term demonstration (10 months) of Test System 2 in wastewater treatment plant effluent.	Accomplished	System was demonstrated at TAU lab with effluent water accomplished by May 2024.	Partially due to delay	Due to delays in reactor development (as detailed above)
<b>M5</b> <b>Fraunhofer</b>	Results of initial LCA	WP7 Ecological evaluation of Test System 2 performance. Sensitivity analysis	Accomplished	Accomplished on Feb 24 for system 1. Initial results for system 2 were completed on July 24 and final results on September 24	Yes	
<b>M6</b> <b>TAU</b>	Evaluations completed and novel evaluation	WP8 Development of scenarios and global	Almost fully Accomplished	Accomplished by September 2024	Yes	The millstone was delayed due to delays in the

	methodology published	impact evaluation (including addressing data gaps in Q7).				technology development as detailed above – for system 2. The feasibility assessment for Germany was not completed due to a lack of data.
--	-----------------------	---	--	--	--	--

**Note: New Milestones – none**

## **Final Scientific Report Covering All Research Years**

### **1. Research Background (0.5 page)**

Micropollutants such as consumer goods, pharmaceuticals and personal care products in water matrices pose significant environmental and human health hazards. Carbamazepine (CBZ), an anti-epileptic and bipolar depression drug, serves as a key micropollutant marker, with studies in Israel and Germany highlighting its prevalence in aquatic environment. The European Union's updated directive now recommends quaternary treatment in wastewater plants to address micropollutants that conventional processes fail to remove. Photocatalytic Membrane Reactors (PMRs) use photon energy, catalysts, and membranes to activate advanced oxidation processes used to degrade micropollutants by generating hydroxyl radicals. This research upgrades PMR technology by developing the CatMemReac reactor, tested at lab and pilot scales for CBZ degradation. A novel feature of this reactor is its use of nickel foam, a highly porous, robust, and cost-effective substrate coated with nanoparticles that are electrically conductive, relatively cheap, and very robust. The incorporation of LEDs aims to reduce the reactor's energy and carbon footprint, compared to ozonation and adsorption. A life cycle assessment (LCA) evaluated the environmental impacts of lab, pilot, and prospective LCA industrial-scale reactors, simulating parameters at technology readiness level 9 (TRL-9). The research shows effective degradation of CBZ by CatMemReac reactor in the lab and the improvement in treatment upon the development of a pilot-scale reactor setup. While the CatMemReac shows higher greenhouse gas emissions compared to alternatives, the study identifies opportunities for improved sustainability. This research demonstrates effective CBZ degradation and provides a comprehensive assessment of the technology's environmental and operational potential.

### **2. Research Methods and Findings (2 pages)**

The aim of the research was to develop a photocatalytic reactor (PCR) for degradation of micropollutants in water by immobilizing a catalyst onto a highly porous substrate and integrating it

into the PCR. The chosen substrate is Nickel foam, having a 200-600  $\mu\text{m}$  pore size and high electrical conductivity that allows coating via the electrophoretic deposition (EPD). EPD cells and electrodes were designed and manufactured, and the coating process was examined for optimal results. A few catalysts were synthesized, such as g- $\text{C}_3\text{N}_4$ , N-doped  $\text{TiO}_2$ , and commercial  $\text{TiO}_2$ , and commercial  $\text{TiO}_2$  was chosen. The Ni foam coated by commercial  $\text{TiO}_2$  ( $\text{TiO}_2$ -Ni) was characterized by XRD, SEM-EDS, streaming zeta potential, XPS, ESR, DRS, and permeability, placed in a PCR and irradiated by UV-A LEDs ( $365 \pm 10 \text{ nm}$ ). Carbamazepine (CBZ) was selected as a probe pollutant, with its removal quantified via HPLC-MS. Experiments optimized removal and energy efficiency by testing flow rates, irradiation intensities, exposure times, pH levels, and wavelengths. Under optimal conditions, a removal rate of  $787 \text{ nmol L m}^{-1} \text{ s}^{-1}$  or 80% removal (WP2+4).

Effluents spiked with CBZ were tested to evaluate removal and characterize reaction engineering parameters (WP2). Methylene blue was used for literature comparison and chemical engineering applications like online kinetics detection. Dimensional analysis identified volume flow (equivalent to irradiation time) as a key parameter, leading to the selection of four flow rates monitored over 200 minutes for distinct degradation rates. Key tools such as actinometry, free radical detection (scavenging potential), and residence time distribution were adapted to the system to determine figures of merit before upscaling. Two recalcitrant X-ray contrast media species were selected as target pollutants for degradation experiments. These pollutants were spiked into distilled water, tap water, and wastewater under varying irradiation times. The wastewater, sourced from the German Büsnau treatment plant after the third treatment step, simulated the potential application of CatMemReac as a fourth-stage alternative. As reflected in the project's title on solar-driven processes, a new lab-scale reactor was designed and built to enable direct solar irradiation and testing of visible light panel emitters (OLEDs). The findings were supported by reaction engineering characterization to establish meaningful figures of merit for future scale-up (WP3).

The pilot scale reactor and  $\text{TiO}_2$ -Ni EPD coating cell were designed based on the lab-scale systems improvements to minimize organic solvent and chemical waste, enabling the coating of  $24.5 \times 18 \text{ cm}^2$  Ni foam. The reactor was optimized for balanced water flow, minimal stagnation, reduced light-catalyst throw distance, and minimal water between the light source and catalyst. The system includes six reactors, each with a  $24.5 \times 18 \text{ cm}^2$   $\text{TiO}_2$ -Ni, configurable in series (6 reactors) or two sets of three, varying from 1 to 6 reactors per setup. To utilize transmitted photons, the reactor is made of reflective aluminum, with PMMA plates ( $\sim 90\%$  UV-A transmittance) replacing fragile quartz. Retention times showed the pilot scale required  $\sim 4$  minutes versus 120 minutes for the lab scale to achieve 80% removal. Net retention times were 1 minute (pilot) versus 3.1 minutes (lab). Reactor efficiency in CBZ degradation was tested across flow rates, wavelengths, and water matrices (DI, groundwater, SAT, effluent), including lower CBZ concentrations to mimic real water sources (WP 5+6).

We conducted a life cycle assessment (LCA) of the CatMemReac technology following ISO 14040 standards to estimate its global warming potential (GWP) for micropollutant removal,

specifically targeting CBZ. The functional unit of the assessment was 1 m<sup>3</sup> of water treated by CatMemReac technology, same for both scales. The system boundary included the operational phase input components as pumps, nickel foam, EPD, and LEDs. The LCA was performed in the OpenLCA 2.0.0 software with the Ecoinvent database (Ecoinvent 3.9.1). The life cycle inventory was developed by working with the technical team at TAU. The background data inventory was adopted from the Ecoinvent database, widely adopted commercial database for LCA. The background data inventory for some components was developed using data from literature/patents. The life cycle impacts were determined using the ReCiPe 2016 v1.03, a mid-point approach that uses IPCC models for global warming potential characterization factors.

The GWP estimates for the lab and pilot scale setups at 1000 ppb CBZ concentrations were 3492.03 kgCO<sub>2</sub>eq/m<sup>3</sup> and 86.53 kgCO<sub>2</sub>eq/m<sup>3</sup>, respectively. Similar significant difference were observed for the 20 ppb and 5 ppb CBZ concentrations. The GWP for 5 ppb was lowest at 15.85 kgCO<sub>2</sub>eq/m<sup>3</sup> for the pilot-scale setup. This variation in GWP is attributed to differing operational times between lab and pilot-scale setups. The pilot-scale setup achieved reduced operation times due to design parameter changes, including increased surface area. Electricity use contributed 99% of total GWP. The major uses of electricity in the setup were chiller, LEDs, pump, and sensors, contributing to 33%, 29%, 23%, and 15%, respectively (for 5 ppb CBZ treatment), while the consumables in nickel foam and EPD setup contribute insignificantly. To ensure the sustainable operation of reactor setup, a sensitivity assessment was performed by modeling the cleaning of Ni foam after 40 cycles of water treatment. H<sub>2</sub>O<sub>2</sub> treatment was recommended as it enhances the longevity of nickel foam and has a relatively low GWP. To enhance the robustness of the LCA results, the uncertainty assessment was also performed using the Monte-Carlo simulation approach.

Based on the results for the lab and pilot scale, we also performed a prospective life cycle assessment of the industrial-scale process of the CatMemReac technology. The futuristic inventory for the industrial-scale setup was developed through interviews and workshops with technology developers team as well as interviews with external experts. The prospective LCA calculated the GWP of 2.2 kg CO<sub>2</sub>eq/m<sup>3</sup> for the best-case industrial-scale scenario of the CatMemReac technology. The CatMemReac team recommends exploring the use of the technology for decentralized groundwater and wastewater reuse applications, as its scalability overcomes the operational and handling constraints that hinder competitive technologies as ozonation.

### **3. Future Research Directions, Applications of Research, and Plans for the Future**

- Partnering with commercial manufacturers of metal or ceramic foams in the coating-substrate axis can facilitate the production of TiO<sub>2</sub> foam, eliminating the coating step and enabling the creation of a more durable material.

- Conducting long-term operations on an existing platform (e.g., Shafdan) will help demonstrate the technology's functionality, identify potential flaws, and support its advancement.
- Update Life Cycle Assessment (LCA) data based on the operation of a larger system.

#### **4. Conclusions and Operational Recommendations (if applicable)**

Further research into a wider range of water contaminants and water qualities and long term demonstration—will help establish the limits of the technology's capabilities. The study showed the GWP based on the LCA of lab and pilot scale setup of CatMemReac technology for the degradation of CBZ. The lab scale setup exhibits high global warming potential GWP. Upon improvement in the design, which includes an increase in surface area of nickel foam and system design reduces the reaction time from 100.6 minutes to 3.9 minutes for degrading 5 ppm CBZ in lab and pilot scale setup, respectively. The main contributor to the GWP was electricity use in pumps and LEDs. The sensitivity analysis showed 96% reduction in GWP for the greener electricity grid mix compared to the Israeli mix for the CatMemReac. The magnitude of the value for the greener mix is 0.6 kgCO<sub>2</sub>eq/m<sup>3</sup> which is twice as reported for Ozone treatment and has potential to be reduced with further development in the CatMemReac technology.

#### **5. Detailed Division of Work Between Partners Based on the Work Plan**

The previously described work packages are assigned based on research group responsibilities: Fraunhofer IGB (1 and 3), TAU Technical Group (2, 4–6), Fraunhofer ISI and TAU LCA team (7), and the TAU LCA Team (8).

#### **6. Details of Meetings Between Researchers or Their Teams (Visits, Work Meetings, Student Exchanges, etc.)**

- Quarterly update meetings of all researchers took place on a constant basis.
- An LCA workshop was held at the beginning of the first year of the research so the technical teams could better understand the LCA teams' needs and roles.
- The research groups conducted bi-weekly meetings to update each other, share data and knowledge, discuss problems, and consult with each other.
- Dr. Benjamin Wriedt (Fraunhofer IGB) visited TAU in October 2022, and Amit Imbar (TAU technical group) visited Fraunhofer IGB in August 2023. Both visits allowed hands-on knowledge sharing and the conduct of experiments.
- Team members from TAU and Fraunhofer visited Germany to present the progress of the research work in the German-Israeli Cooperation in Water Technology Research Status Seminar in June 2024. The presentation included the research work for CatMemReac development done by TAU and Fraunhofer. The presentation also showed the progress of CatMemReac research.

- The LCA teams worked closely together and shared files and results as well as consulting with local experts etc

## **Appendix**

### **TAU Technical team**

#### **1. Material and methods**

##### **1.1. Chemicals**

For the coating process, Ni foam (Ni-4753.03) was obtained from Recemet (Dodewaard, The Netherlands); TiO<sub>2</sub> powder product (Germany, CAS 13463-67-7), and Zinc Nitrate (reagent grade 98) were both provided by Sigma Aldrich. Carbamazepine (CBZ) was used as a target pollutant (Sigma-Aldrich, analytical standard).

##### **1.1.1. Carbamazepine stock solution**

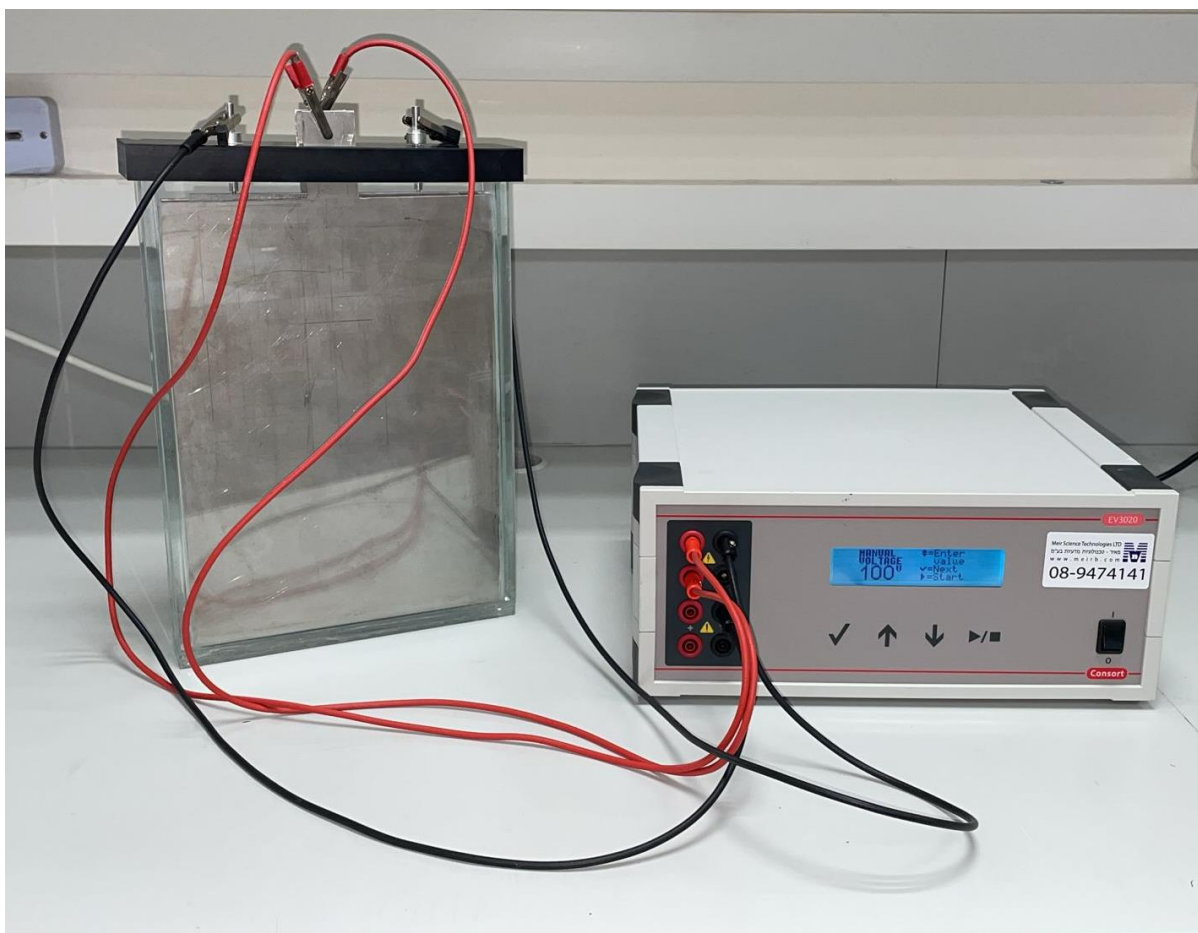
25 mg of CBZ was dissolved in 500 mL of Deionized (DI) water, forming a 50 ppm CBZ stock solution. Working solutions were made by diluting the stock solution in DI water to a concentration of 1 ppm. For specific experiments, further dilution to 20 ppb was done by diluting the 50 ppm solution to 1 ppm, following a second dilution of 1 ppm solution to 20 ppb with pH adjustment to 7. The pH of the working solutions was adjusted to 7 using a sodium phosphate monobasic and sodium phosphate dibasic mixture (Phosphate Buffer, PB) in 1 mM concentration<sup>1</sup>.

##### **1.2. Fabrication of TiO<sub>2</sub>-Ni foam**

Ni foam was coated with a commercial TiO<sub>2</sub> via an EPD approach<sup>2</sup>. The TiO<sub>2</sub> was heat treated for 2 hours at 450 °C to remove any impurities. The EPD cell had two stainless steel counter electrodes placed at a 10 mm distance from the target electrode. Ni foam was immersed in IPA for cleaning purposes, followed by air pressure drying. A suspension of 4.33 gr L<sup>-1</sup> of TiO<sub>2</sub> and 0.4 gr L<sup>-1</sup> Zn(NO<sub>3</sub>)<sub>2</sub>·6H<sub>2</sub>O in IPA was sonicated for 15 minutes and stirred. The suspension and Ni foam were placed in an EPD cell. The coating process was set for 5 minutes. After 5 minutes, the solution was stirred and set for another 5 minutes. The obtained TiO<sub>2</sub>-Ni foam was dried in ambient conditions.

The EPD cell is a custom-made glass cell with inner dimensions of 200x25x290 mm<sup>3</sup> glued with IPA resistive glue. The lid, including the arm that holds the Ni foam, is a custom-designed and manufactured prototype. The setup is shown in Figure 1.





*Figure 1: Large-scale EPD cell and power supply.*

### **1.3. Analytical methods and instruments**

Scanning Electron Microscopy (SEM) was conducted with a Thermo Fisher Quanta 200 FEG ESEM instrument. Crystallinity was analyzed using a powder x-ray diffractometer (XRD) by Bruker D8 Discover diffractometer with the linear energy discriminate detector LINXEYE XE operating with Cu-K $\alpha$ 1 radiation ( $\lambda = 1.54 \text{ \AA}$ ) at a scan rate of  $3^\circ \text{ min}^{-1}$  and a 2 theta range of  $5\text{--}70^\circ$ . Zeta potential was measured by an Anton Paar SurPASS 3 instrument using 0.001 M KCl. EPR spectra were recorded on a Bruker ELEXSYS E500 X-band spectrometer equipped with a Bruker ER4102ST resonator in a Wilmad flat cell for aqueous solutions (WG-808- Q) at room temperature. Light excitation was done using a (Schott KL 1500 lamp) which is a 150-watt halogen cold light source. Experimental conditions were 512 points, with a microwave power of 20 mW, 0.1 mT modulation amplitude, and 100 kHz modulation frequency. The sweep range was 20 mT. To probe the optical properties of the prepared photocatalysts, UV–visible diffuse reflectance spectra were recorded using a UV–Vis–NIR spectrophotometer (Cary 5000 + UMA, Agilent, Santa Clara, CA, USA). Water transmittance

was recorded using Evolution 220 UV-visible spectrophotometer by Thermo Scientific.

#### 1.4. Light source

Custom-made LED arrays were used as light sources during the research, with 365 and 405 nm wavelengths. All the LED arrays were designed and manufactured by Violumas Inc. (Fremont, CA, USA) and Boston Electronics (Brookline, MA, USA). Measured emission spectrums and incident irradiance values are shown in Figure 2 and Table 1.

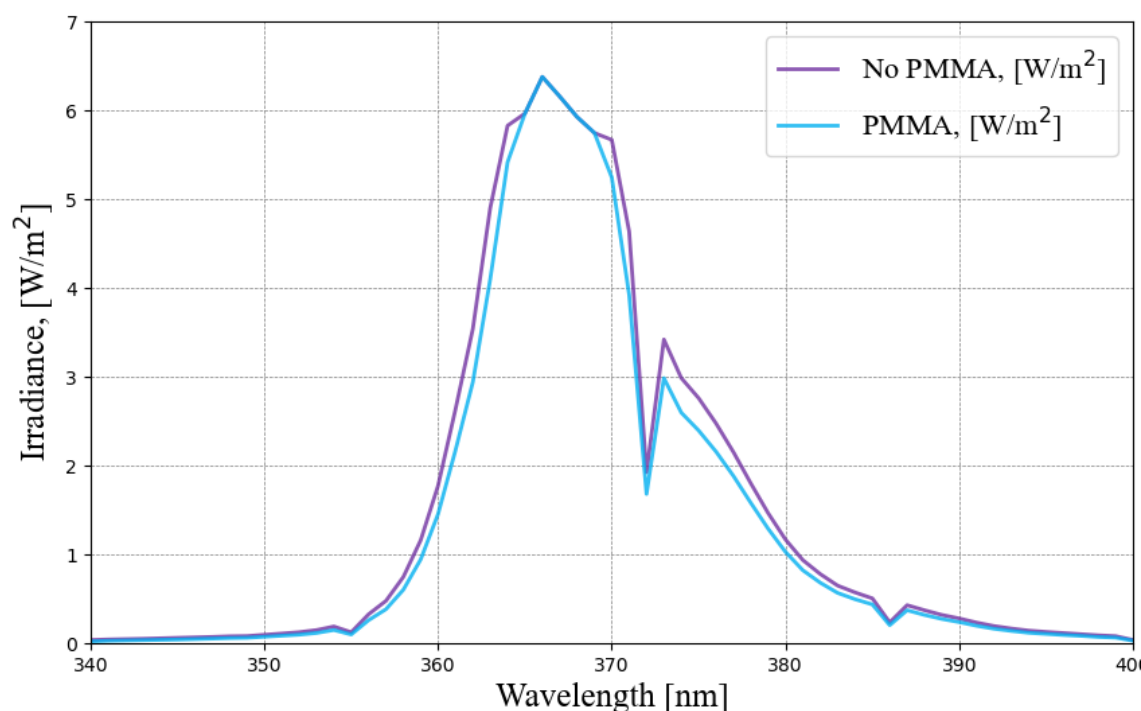


Figure 2: Emission spectrum of 365 nm LEDs, under PMMA cover (purple), and without PMMA cover (blue). All measurements were taken at a throw distance of 35 mm

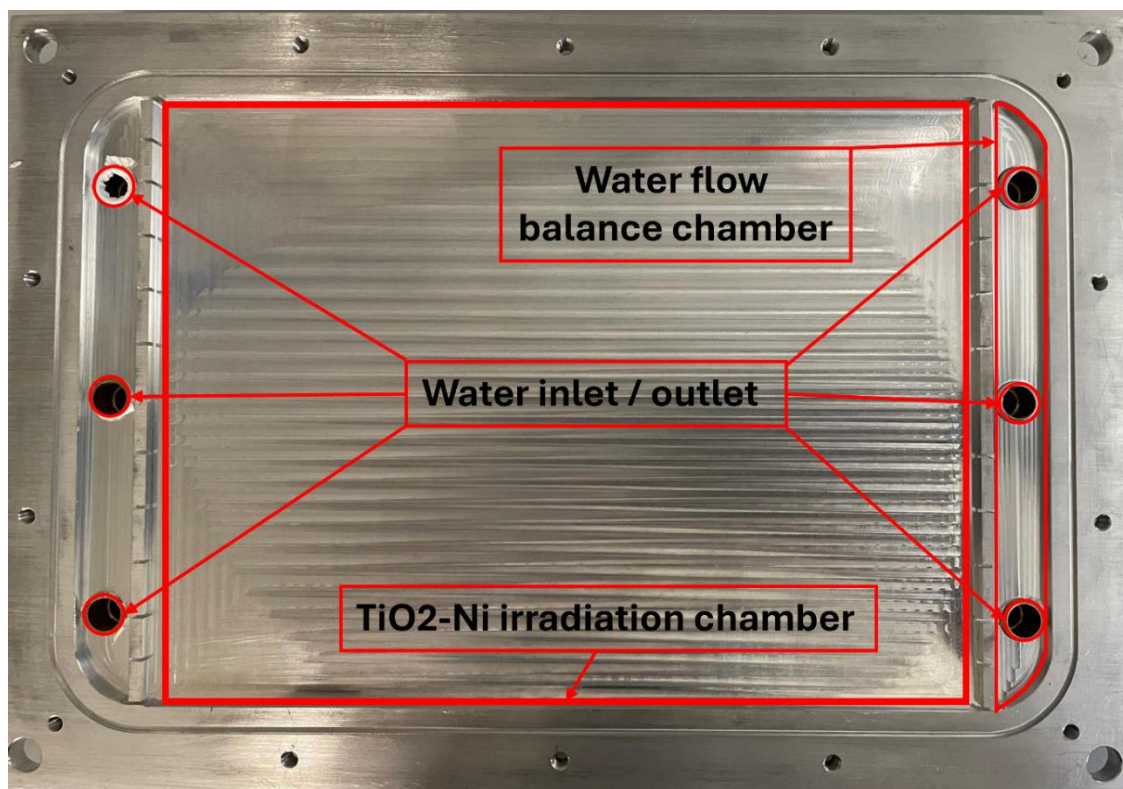
Table 1: Summarized values of measured incident irradiance of three LED plates, 365 and 405 nm.

LEDs [nm]	365	
	365	under PMMA
Input power [W]	36.3	36.3
Incident Irradiance [W/m <sup>2</sup> ]	91.09	82.13

#### 1.5. Pilot reactor design

The reactor was designed under the following guidelines: first, it has a sizeable irradiated area (vs. the lab scale) to increase the number of active catalytic sites, providing more reactive

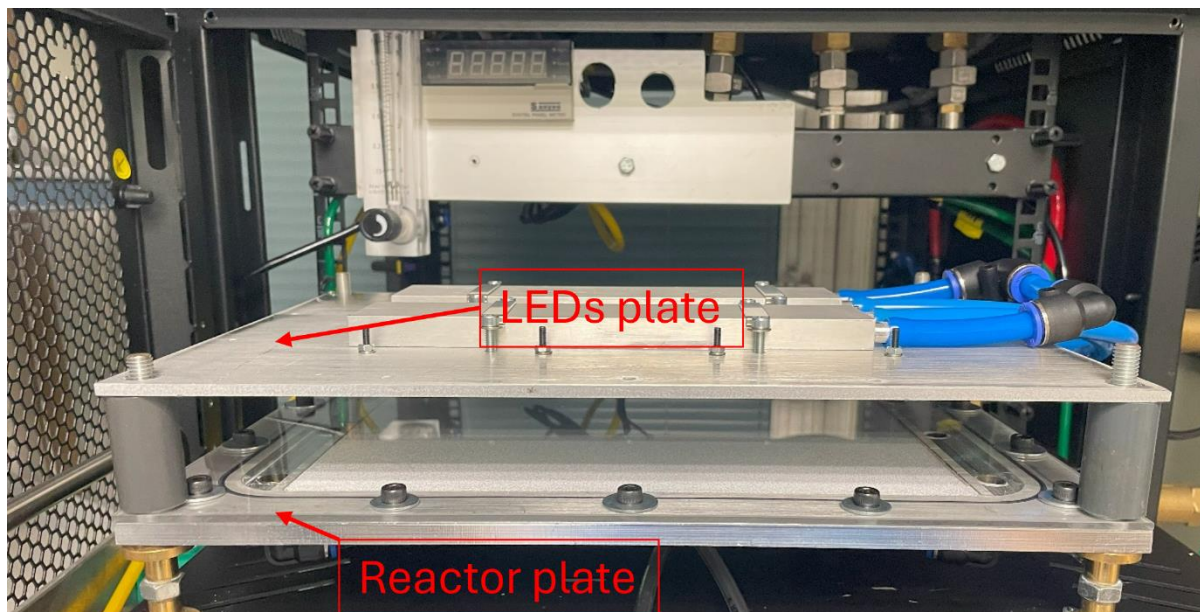
oxidative species (ROSs). The second and most important is maximizing the utilization of the photons delivered by LEDs to the catalytic sites. This objective, from the perspective of reducing CO<sub>2</sub> emission reduction, is the most crucial since LEDs are the primary energy consumer in the process. To that end, the throw distance of the LEDs (the distance between the LED and the target) and the water level above the TiO<sub>2</sub>-Ni were minimized. The material from which the reactor is made is aluminum; it was chosen due to its reflectivity, allowing the utilization of photons passing through the TiO<sub>2</sub>-Ni all the way down. Moreover, the cover material that seals the reactor is not quartz due to its fragility but a UV transparent (~90% transmittance at 365 nm LEDs) material. Third, in order to maximize the photoactivity of the irradiated catalytic sites, the water flow had to be as even as possible on all parts of the TiO<sub>2</sub>-Ni and avoid stagnation points. Figure 3 shows the reactor from a top view. The reactor has three inlet/outlet holes, flowing water into a flow balance chamber at which the water pressure equalizes, providing equal water flow over the TiO<sub>2</sub>-Ni pores. The TiO<sub>2</sub>-Ni chamber is where the TiO<sub>2</sub>-Ni is placed. Around the chambers and inlet/outlet holes, unmarked, is the rubber seal trench. A PMMA plate covers the entire aluminum plate on top.



*Figure 3: Picture of an empty reactor. Made of aluminum, has three inlets and outlet holes, a reaction chamber for the TiO<sub>2</sub>-Ni, and a water flow balance chamber.*

For future work, the complete setup was designed to contain six units that can operate either in a one-column row of 6 reactors or two columns of 3 reactors. Figure 4 presents one unit of

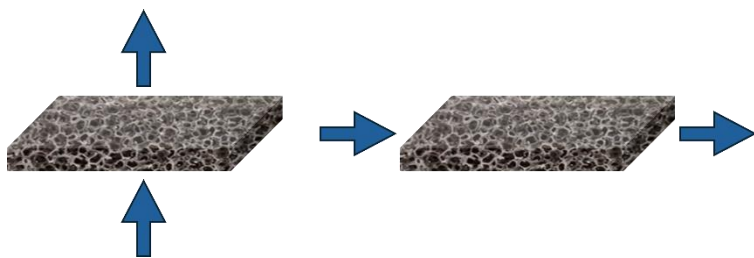
reactor and LEDs.



*Figure 4: A single reactor (bottom plate ) and LEDs (top plate) unit assembled. The blue pipes on top are for cooling water.*

#### **1.6. CBZ degradation in a photocatalytic (PC) reactor**

The degradation efficiency of the upscaled reactor unit was examined by placing a Ni foam sheet of  $18 \times 24.5 \text{ cm}^2$  ( $441 \text{ cm}^2$ ) coated by  $\text{TiO}_2$  in the reactor and irradiating it with LEDs. In the pilot scale reactor, the water flow is cross-sectional, unlike the lab scale, at which the water flows through the Ni foam (flowthrough) Figure 5.



*Figure 5: Flowthrough (on the left) vs. cross-sectional flow (on the right).*

The irradiated area is  $441 \text{ cm}^2$ . All the described experiments were conducted under similar incident irradiance (see Figure 2). The flow rate was controlled by adjusting the peristaltic feed pump. Different water matrices were used to examine the impact of different chemical components on the photocatalytic process. Unless stated otherwise, the volume of treated water is 0.5 Liter, the concentration of CBZ is 1 ppm, and the duration of the experiment was 15 minutes. Every experiment started with a 15-minute equilibration phase by water circulation under dark conditions. After every experiment, the system was washed with DI water, and placed to dry in  $60^\circ\text{C}$ . Each experiment was triplicated for reproducibility. The



same TiO<sub>2</sub>-Ni was used for all experiments. After each experiment, DI water is circulated inside the system to wash the CBZ remnants and other contaminants. After draining all the water, the cover of the reactor was removed, and the entire aluminum plate and TiO<sub>2</sub>-Ni were left to dry for one hour or more at 60 °C.

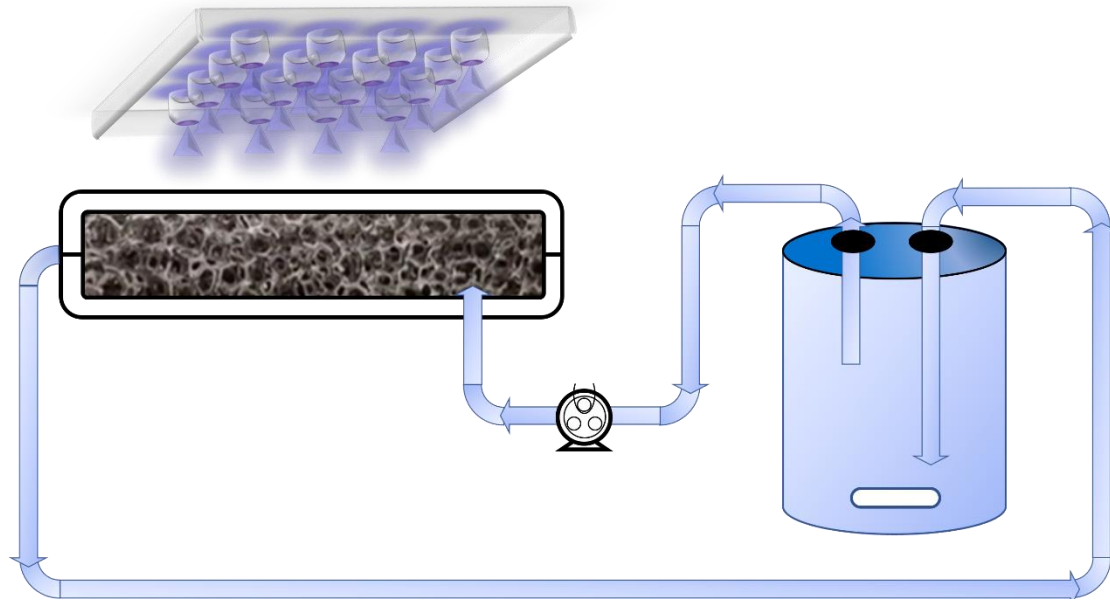


Figure 6: Reactor setup and process scheme.

The removal of CBZ at time  $t$  was calculated from Equation (1):

$$R_t = 100\% \cdot (C_i - C_t) / C_i \quad (1)$$

$C_i$  is the initial concentration of CBZ (1 ppm), and  $C_t$  denotes the CBZ sample concentration at time  $t$ .

### 1.7. Mass spectrometry quantification

The CBZ was detected and quantified by LCMS using a Waters Acquity H class UPLC and SQD2 mass spectrometer. The LC separation was performed with a 2.1X50 BEH C18 1.7 micron column. The injection volume was 0.5  $\mu$ L. The mobile phase composition of Water and MeCN with a flow rate set at 0.5 mL/min. Data acquisition and evaluation were performed using Waters chromatography MassLynx 4.1 software.

## 2. Results and discussion

### 2.1. Characterization

#### 2.1.1. SEM-EDS

Figure 7(a-b) illustrates that the Ni foam features macroporosity and a smooth surface. The pore size of the Ni foam exceeds 500  $\mu$ m. SEM images of TiO<sub>2</sub>-coated foam (Figure 7(c-d)), show that the TiO<sub>2</sub> particles are uniformly and firmly covered onto the Ni foam. Moreover, to confirm that the coating was not restricted to the surface, cross-sectional images for TiO<sub>2</sub>-

coated foam were taken. As shown in Figure 7(e-f), TiO<sub>2</sub> nanoparticles were uniformly electrodeposited across the surface and inside the foams. Successful TiO<sub>2</sub> coating inside the foam and on the surface results in enhanced surface area and exposure to more active sites, which may contribute to the photocatalytic activity. In summary, the electrodeposition method resulted in evenly coated TiO<sub>2</sub> inside and on the surface of the nickel foam with high loading compared to the drop-casting method<sup>3</sup>. Further, SEM-EDS was performed on the film's surface to determine the composition of the Ni-foam and TiO<sub>2</sub>-Ni-foam (Table 2). As expected, Ni-foam mainly contains Ni as it is a metallic nickel foam. An insignificant amount of oxygen could be due to a minor portion of oxidized nickel. The electrodeposited TiO<sub>2</sub>-Ni-foam consists of Ti, Ni, and O elements, confirming the deposition of TiO<sub>2</sub> nanomaterials onto the Ni foam surface. Overall, SEM and EDS results demonstrate the successful deposition of TiO<sub>2</sub> onto the open-cell 3D structure of Ni foam.

*Table 2: Atomic Percentage of elements in Ni-foam and TiO<sub>2</sub>-Ni Foam from EDS analysis.*

	Ni-foam	TiO <sub>2</sub> /Ni-foam
Ni	72.32	13.63
O	2.95	53.32
Ti	--	24.39

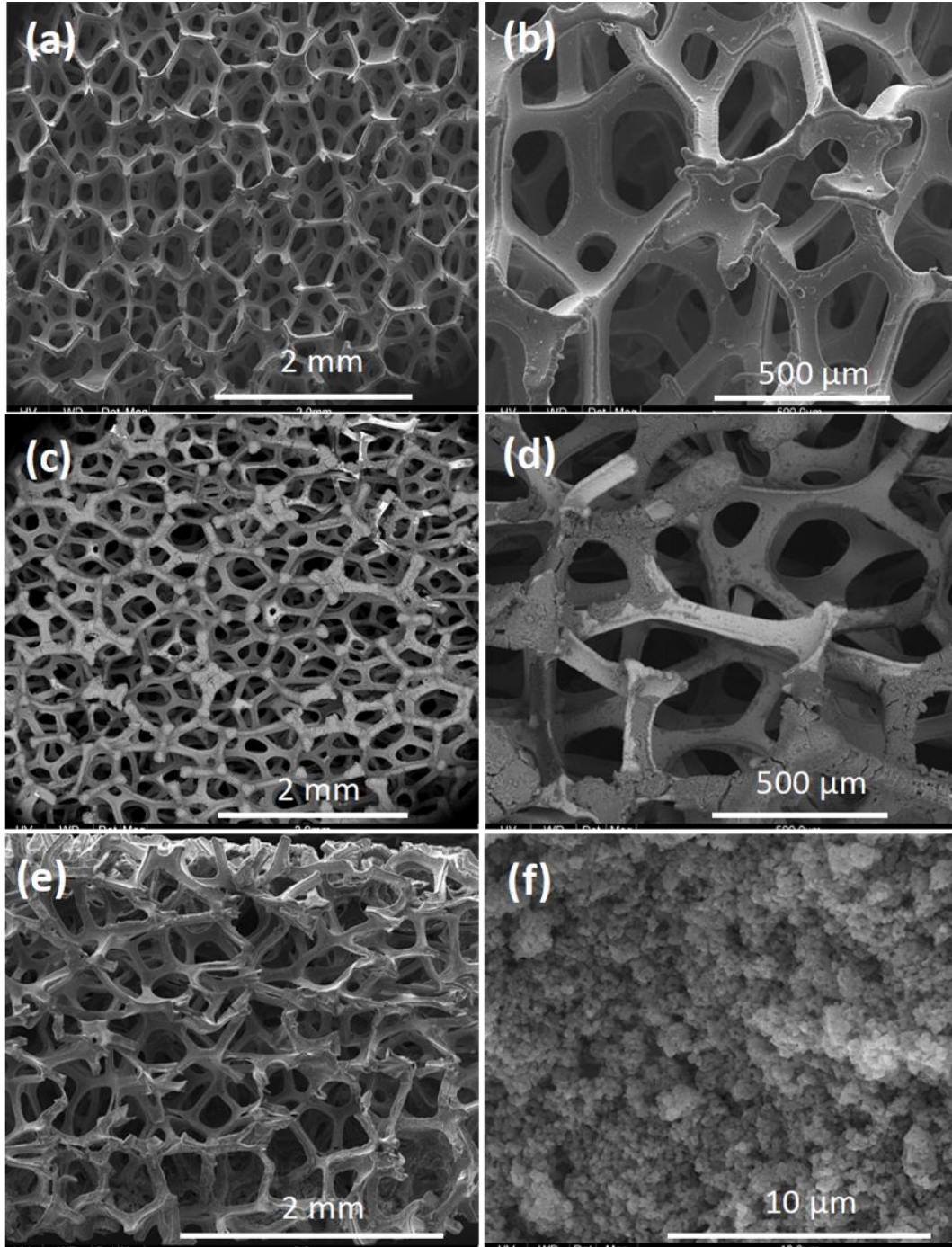


Figure 7: (a-b) SEM images of Ni foam, (c-d) of TiO<sub>2</sub> coated foam, and (e-f) of a cross-section of TiO<sub>2</sub> coated Foam.

#### 2.1.1.1. TiO<sub>2</sub>-Ni coating thickness

The TiO<sub>2</sub>-Ni coating thickness was measured at varying deposition times: 1, 2, 3, 4, and 5 minutes. The coating thickness was determined by SEM images of a cross-cut coated TiO<sub>2</sub>-Ni. To avoid damaging the coating, every sample was partly submerged in resin and left for 24 hours of curing, followed by the cut-off of the non-submerged TiO<sub>2</sub>-Ni and surface

polishing of the resin-TiO<sub>2</sub>-Ni. Each sample was scanned at its edge and center of the TiO<sub>2</sub>-Ni cross-cut, and the coating's thickness was measured at several spots in every image. The measurements from each image were averaged and are presented in Figure 8

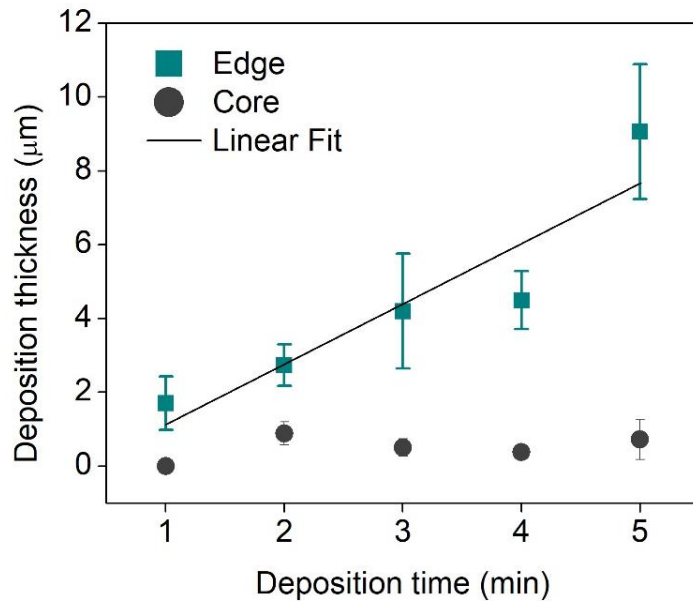


Figure 8: Edge and center deposit thickness [ $\mu\text{m}$ ] of membranes at different deposition times [min].

The thickness of the edge coating shows a linear correlation with 1, 2, and 3 minutes of deposition, which is consistent with the linear form of the Hamaker equation<sup>4</sup>. The deviation of the 4 and 5-minute deposition from the correlation could be explained by changes in the suspended TiO<sub>2</sub> concentration in the TiO<sub>2</sub>-IPA solution during the process<sup>5</sup>, as was observed by Radice et al.<sup>6</sup> and Wang et al.<sup>7</sup>. However, it is worth noting that the linear curve crosses the error bars of the 5-minute edge deposition sample.

The center of the cross-cut coating was much smaller and did not show significant growth with deposition time. This could be explained by the small volume of solution available in the inner pores of the Ni foam. The particles in the bulk solution are assumed to have a stronger attraction toward the edge of the Ni foam than toward the center due to the shorter distance from the bulk to the edge compared to that between the bulk and the center. While the edge of the Ni foam is exposed to the bulk of the solution and to that in the pores, the center is only exposed to the solution in the pores, resulting in a much thinner coating. Figure 9 shows elemental mapping performed by Energy-Dispersive X-ray Spectroscopy (EDS) analysis. A fully continuous and uniform coating of titanium oxide formed on the Ni foam. The migration of atoms from one area to another (Ti atoms from the coating to the Ni or resin, etc.) is a result of polishing.



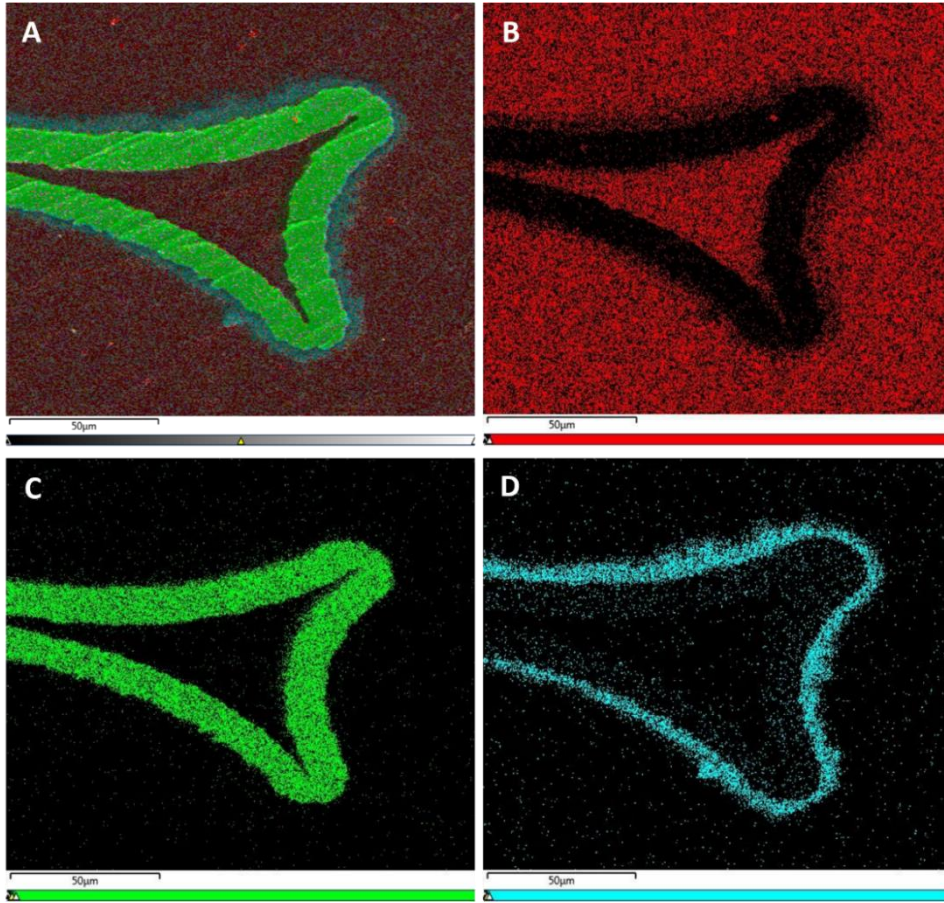


Figure 9: Elemental mapping of  $\text{TiO}_2$ -Ni edge. A- full elemental mapping, B- Carbon (red), C- Nickel (green), D- Titanium (cyan).

### 2.1.2. X-ray diffraction (XRD) analysis

X-ray diffraction (XRD) analyses were utilized to determine the phase structure of Nickel (Ni) foam,  $\text{TiO}_2$  particles, and Ni foam electrodeposited with  $\text{TiO}_2$  (Figure 10a). Distinct peaks identified at 44.8 and 52.2 correspond to the (111) and (200) planes of metallic nickel (PDF#03-1051, cubic crystal structure), respectively. Furthermore, the XRD pattern of heat-treated H- $\text{TiO}_2$  shows characteristic peaks corresponding to diffraction from the (101), (004), (200), (105), (211), and (204) planes (Figure 10a), which are well-matched with the pure anatase phase according to the standard JCPDS card No. 21-1272<sup>8</sup>. Notably, the peaks identified in the XRD analysis that correspond to both the metallic nickel foam and the deposited  $\text{TiO}_2$  particles in the  $\text{TiO}_2$ -Ni foam confirm that the crystalline phase of  $\text{TiO}_2$  remains unchanged after electrodeposition onto the Ni foam. This observation highlights the stability of  $\text{TiO}_2$  under the applied electric field, demonstrating that the deposition process does not induce phase changes. Furthermore, the XRD results indicate that the metallic Ni

foam does not undergo any chemical transformations during the electrodeposition process.

### 2.1.3. Streaming potential

Streaming potential analysis was conducted over a wide pH range to determine the surface charge. Figure 10 illustrates that the metallic nickel foam exhibits a positive charge under acidic conditions attributed to protonation. Upon increasing the pH towards alkaline conditions, a shift from positive to negative Zeta potential was observed, indicative of surface deprotonation and the potential formation of metal hydroxides. Upon electrodeposition of  $\text{TiO}_2$  to the surface of the nickel foam, the Zeta potential of the composite tends to become more negative, attributed to the oxygenated functionalities of  $\text{TiO}_2$  particles. In acidic conditions, the  $\text{TiO}_2$  surface tends to acquire a positive charge due to the protonation of the surface hydroxyl groups. Conversely, in alkaline conditions, the  $\text{TiO}_2$  surface becomes negatively charged as the hydroxyl groups undergo deprotonation, leading to the dominance of negatively charged oxygen species.

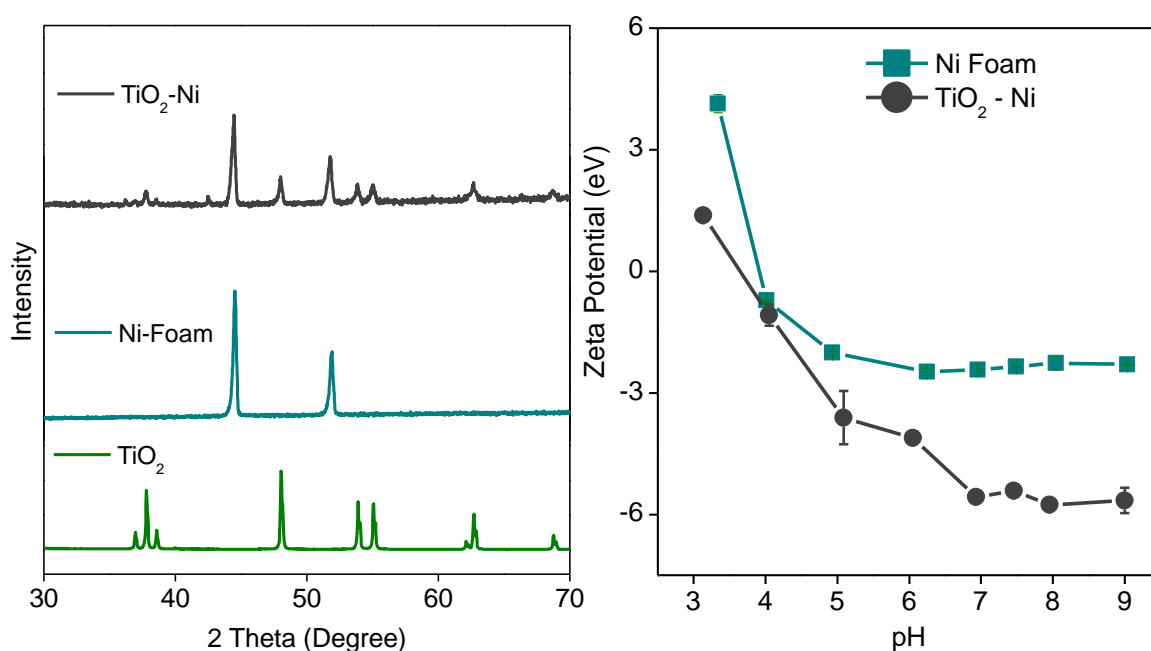


Figure 10: (a) XRD for bare Ni foam,  $\text{TiO}_2$  nanoparticles, and  $\text{TiO}_2$ -coated foam. (b) zeta potential for bare Ni foam and  $\text{TiO}_2$ -coated foam across different pH.

### 2.1.4. X-ray photoelectron spectroscopy (XPS)

The elemental composition and chemical valence of the surface layer of the materials were analyzed using XPS (Figure 11). From the survey spectrum of  $\text{TiO}_2\text{-Ni}$  foam (Figure 11a), the main peaks were identified for oxygen ( $\text{O}1s$ ), titanium ( $\text{Ti}2p3$ ), carbon ( $\text{C}1s$ ) and Ni ( $\text{Ni}2p$ ) at a specific binding energy of 532.16 eV, 459.94 eV, and 287.17, respectively. The specific binding energy at 532.16 eV suggests that oxygen is present as oxides. The  $\text{Ti}2p3$

peak indicates the presence of titanium, typically in the +4 oxidation state, consistent with  $\text{TiO}_2$ . Further, from the deconvolution of the peaks in Figure 11b, the lower binding energy peak at 458.5 eV corresponds to  $\text{Ti } 2p_{3/2}$ , and the higher binding energy peak at 464.4 eV corresponds to  $\text{Ti } 2p_{1/2}$ . From Figure 11c, the lower binding energy peak at 529.7 eV is often associated with oxygen in  $\text{Ti-O}$  bonds. A higher binding energy peak at 531.7 eV is associated with the surface hydroxyl groups<sup>9</sup>. From the deconvoluted  $\text{Ni}2p$  spectrum (Figure 11d), the peaks at lower binding energies correspond to metallic nickel, whereas the peaks at higher binding energies may indicate oxidized nickel species, possibly in the form of nickel oxide, but in low quantity. Thus, the XPS analysis confirmed the successful  $\text{TiO}_2$  coating on the foam's surface and the absence of chemical interaction between  $\text{TiO}_2$  and foam substrate.

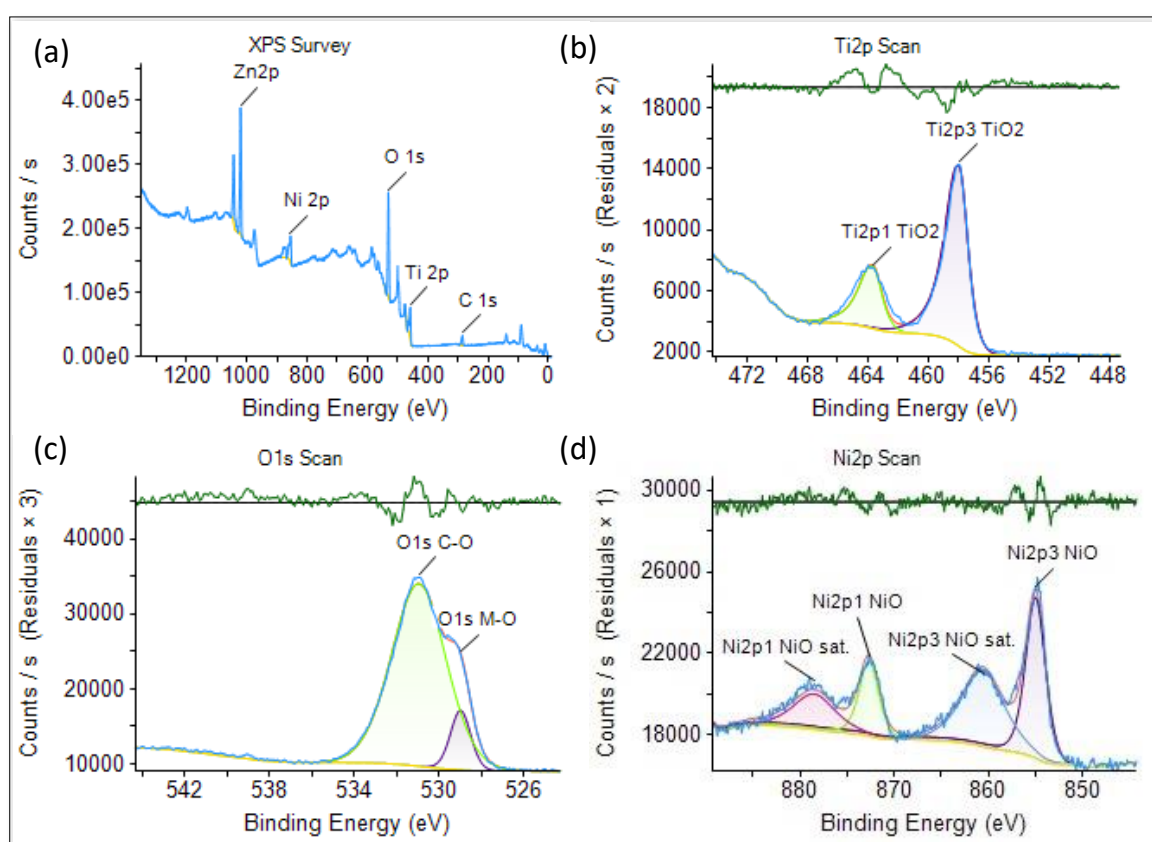


Figure 11: XPS survey spectrum of (a)  $\text{TiO}_2$ -Ni foam, (b)  $\text{Ti}2p$ , (c)  $\text{O}1s$ , and (d)  $\text{Ni}2p$  XPS spectra of XPS survey spectra of  $\text{TiO}_2$ -Ni foam.

### 2.1.5. Electron spin resonance spectroscopy (ESR)

ESR spin trap (also known as EPR, Electron Paramagnetic Resonance) experiments were conducted to study the formation of ROS over  $\text{TiO}_2$  when exposed to a broad light spectrum, similar to those reported by Kumar et al.<sup>10</sup>. An aqueous suspension of  $\text{TiO}_2$  was irradiated under solar light in the presence of 5-methyl-1-pyrroline N-oxide (BMPO), which reacts with

both  $\cdot\text{OH}$  and  $\cdot\text{O}_2^-$  radicals. To differentiate the signal related to  $\cdot\text{OH}$  radicals from those of  $\cdot\text{O}_2^-$  radicals, dimethyl sulfoxide (DMSO), known as an  $\cdot\text{OH}$  radical scavenger, was added to the  $\text{TiO}_2$ -BMPO suspensions. The signals obtained are shown in Figure 12. In the  $\text{TiO}_2$ -BMPO solution, the ROSs (either  $\cdot\text{OH}$  or  $\cdot\text{O}_2^-$ ) produced by the irradiation reacted with the BMPO to form an inconsistent intensity of signals (low-high-high-low) corresponding with  $\cdot\text{OH}$  radicals. The addition of DMSO eliminated the BMPO- $\cdot\text{OH}$  reaction, resulting in a prominently lower signal than the solely BMPO suspension, fluctuating close to the horizontal axis. The inconsistency of the BMPO solution signal peaks and the weak signal resulting from the DMSO suspension suggest that  $\cdot\text{O}_2^-$  radicals are not formed on the  $\text{TiO}_2$  catalyst, but only  $\cdot\text{OH}$  radicals are produced. The ROS produced during  $\text{TiO}_2$ -assisted photocatalysis will interact with CBZ during the photocatalysis.

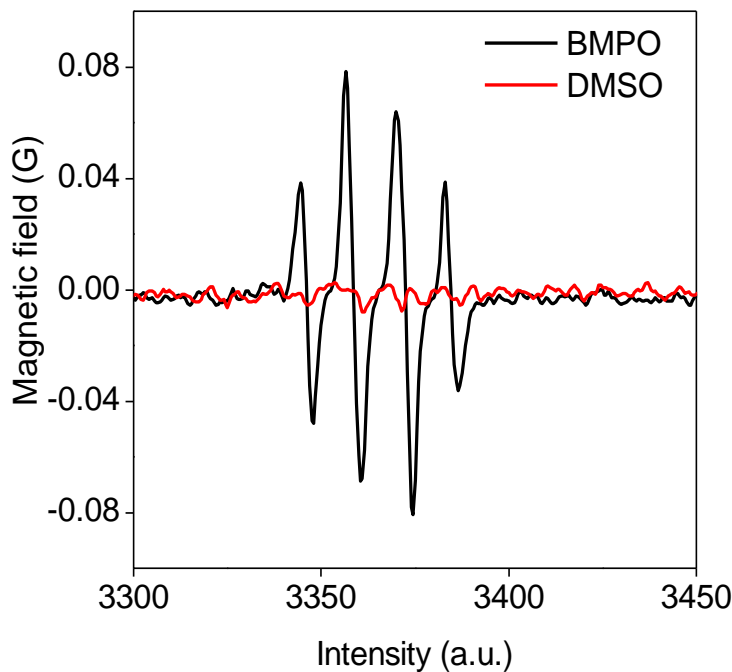


Figure 12: BMPO- $\cdot\text{OH}$  with (black line) and without (red line) DMSO signal from the suspended  $\text{TiO}_2$ .

Therefore, the generation of ROS during photocatalysis with  $\text{TiO}_2$  nanoparticles can be described by the following Equations (2-6):



These findings are important mainly because  $\cdot\text{OH}$  radicles are second only to fluorine in terms

of oxidation potential (2.8 vs. 3.03 eV, respectively)<sup>11</sup>, and is significantly higher than that of ozone, 2.07<sup>12</sup> and therefore is capable of removing a wider range of contaminants.

## 2.2. Flow rate impact on degradation

In a continuous flow setup, the degradation of CBZ is dependent on the flow rate. In embedded catalyst configuration, the reduced surface area for reactant-catalyst reaction results in a decrease in the generation of ROSs. On the lab scale experiments, the impact of flow rate was demonstrated (presented in Figure 13). Five flow rate values were tested, showing a maximum removal rate and a decrease in removal as the flow rate is further increased or decreased, similar to the results observed by Ferná'ndez et al<sup>13</sup>.

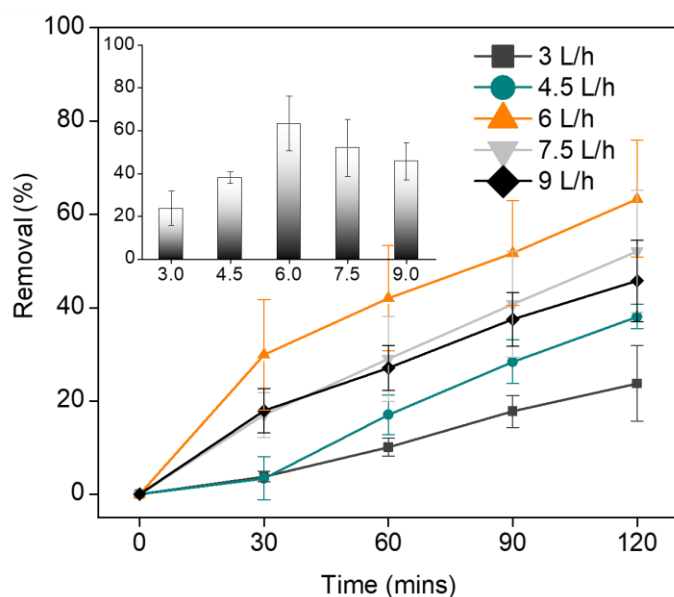


Figure 13: CBZ removal in a lab-scale reactor under varying flow rates. The bar chart shows the total removal after 120 minutes of irradiation.

Similar experiments were conducted on the pilot reactor to maximize CBZ removal. Three Flow rats were tested: 20, 40, and 60 LPH, under similar conditions as described In section 1.6. The results are shown in Figure 14.

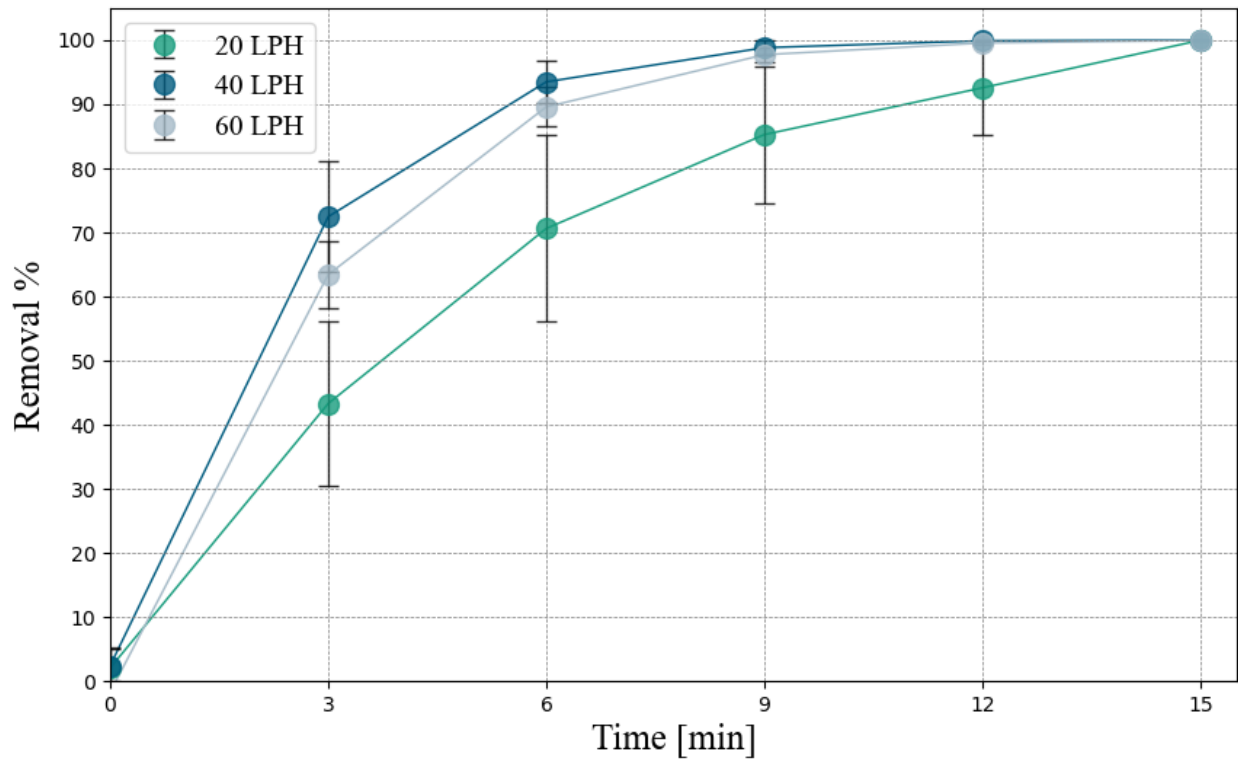


Figure 14: CBZ removal vs. time, under varying flow rates.

All experiments showed 100% removal after 15 minutes. However, the 20 LPH flow rate is the least efficient of the three. Moreover, the results obtained by the 20 LPH flow rate have wide error bars, which indicate an unstable process. The difference between 40 and 60 LPH is smaller, seen mainly in the 3 and 6 minutes, with an advantage toward 40 LPH. For 40 LPH, 9 minutes shows the total removal of CBZ, while for 60 LPH, it was 12 minutes. These experiments, at which the retention time was constant, but the flow rate varied, along with the experiment conducted over the lab scale reactor, show that not only the retention time (e.g., time of exposure to irradiation) plays a crucial rule, but also mass transfer has its.

Based on the 40 LPH data, a linearized form of a first-order kinetic equation was plotted to calculate the removal of 80% (where the rate constant  $k$ , the slope, is 0.539 [1/min], and  $C/C_0=0.2$ ).

The developed form of the first-order is shown in Equation 7:

$$-dC/dt = kC \quad (7)$$

The linearized form of the first-order kinetic equation is shown in Equation (8):

$$-\ln(C/C_0) = kt \quad (8)$$

$C_0$  denotes the initial concentration, and  $C$  denotes the concentration of CBZ in different time sampling (it is the dependent variable).  $k$  is the reaction rate constant (slope, 0.539 [ $\text{min}^{-1}$ ]), and  $t$  is the time in minutes (independent variable).

The results of the calculation of the retention time required to remove 80% CBZ (using the linearized form of first-order kinetic with  $k=0.539$ ) is ~3 minutes, which is not the same as the measured removal at 3 minutes (measured 72% removal). Since, after 6 minutes, the removal was over 95%, the assumption is that after 4 minutes, the removal was over 80%. Based on that, an actual retention time calculation was made, as shown in section 2.3.

### **2.3. Retention time - lab vs. pilot scale**

According to Equation 9, to reach 80% removal of CBZ, the actual retention time in the pilot reactor is approximately one minute (vs. 3.1 minutes with the lab scale, less than a third). This was determined by dividing the reaction volume ( $V_r$ , ~125.7 mL) by the total volume ( $V_t$ , total volume of water treated, 500 mL), multiplied by the duration of the experiment ( $t_{exp}$ , 4 minutes needed to reach over 80% removal according to section 2.2). The reaction volume was defined as the volume of  $TiO_2$ -Ni pores volume, a multiplication of irradiation area ( $A$ , 441  $cm^2$ ) by the Ni foam thickness ( $h_f$ , 0.3 cm) and the porosity ( $\phi$ , 0.95).

$$t_{ill} = (V_r/V_t) \cdot t_{exp} = ((A \cdot h_f \cdot \phi)/V_t) \cdot t_{exp} \quad (9)$$

### **2.4. Experimental-based calculation of required irradiation time**

Calculating the required irradiation time is based on the removal requirements, which are 80% out of 5 ppb (final concentration of 1 ppb), as was set by the European standard. However, due to instrument resolution limitations, measuring these low concentrations was not possible. To overcome that, a 20 ppb solution was used to model the removal at a concentration as close as possible to the desired 5 ppb. The solution was treated for 15 minutes, similar to the description in section 1.6. The results were linearized using the first-order kinetic equation shown previously, and the required irradiation time (under the current conditions) was determined.

The data of  $\ln(C/C_0)$  vs. time was plotted (in blue) based on the developed kinetic equation, showing linear form, as can be seen in Figure 15.



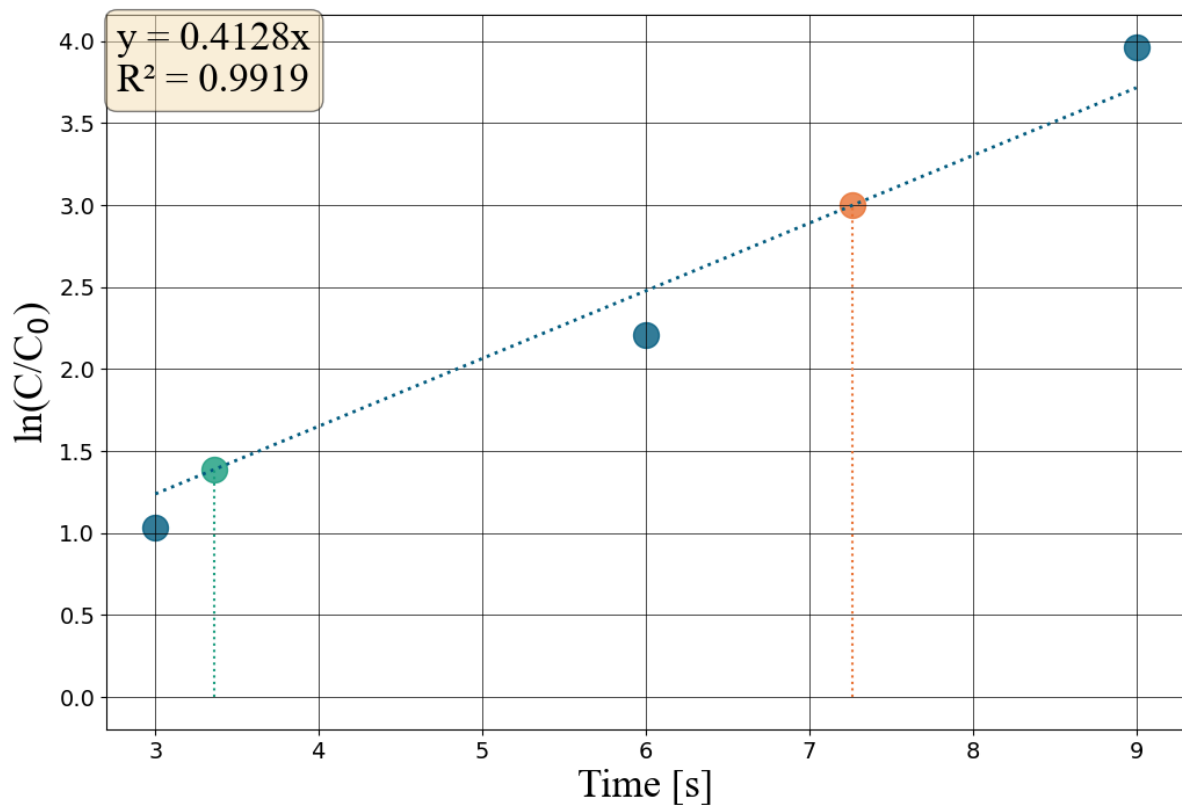


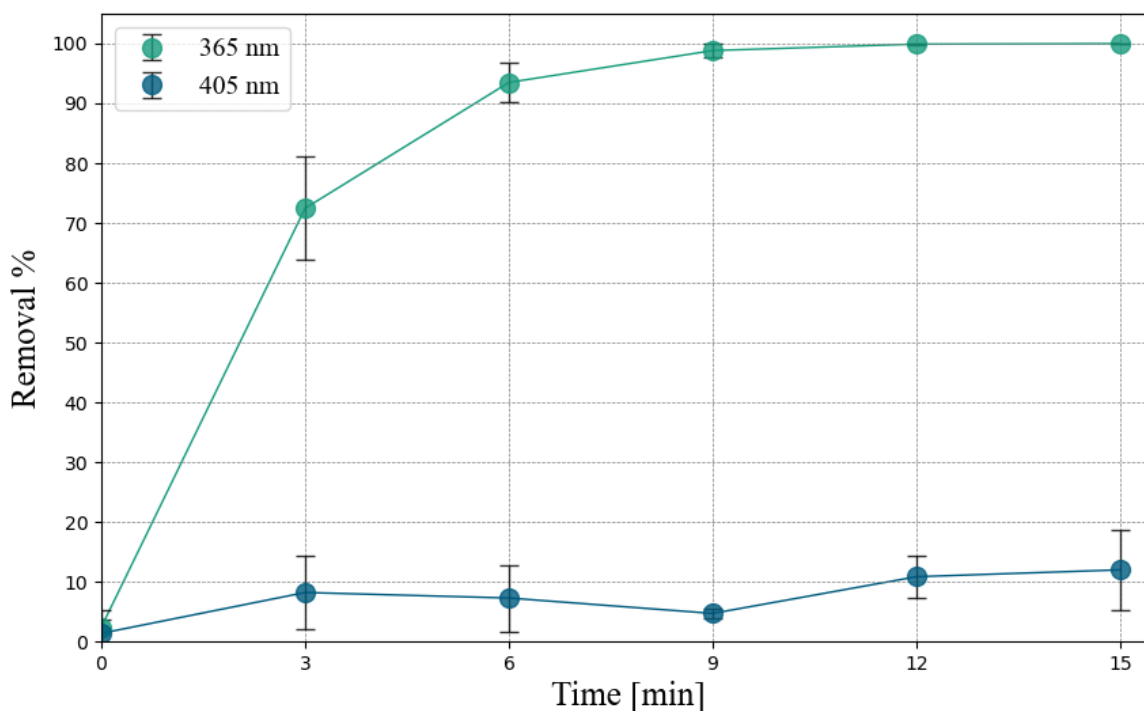
Figure 15: Plot of 20 ppb CBZ removal over linearized form of first-order kinetic equation (in blue). The green marker is the time at which  $C=5$  ppb and the orange marker is the time at which  $C=1$  ppb.

Since the initial concentration is 20 ppb rather than 5 ppb, the time required to reduce it from 20 ppb to 5 ppb, 3.36 minutes (green marker, 3 minutes and 22 seconds), was subtracted from the time required to reduce it from 5 ppb to 1 ppb, 7.26 minutes (in orange, 7 minutes and 15 seconds), summing to 3.9 minutes (3 minutes and 54 seconds). According to these findings, the technology could be better assessed by LCA.

## 2.5. Impact of wavelength

LEDs and other light sources are inefficient in terms of electricity utilization, producing mainly heat rather than photons. Generally, photons of longer wavelengths carry less energy and, therefore, can overcome narrower bandgaps of photocatalysts. On the other hand, LEDs of longer wavelengths are more efficient, e.g., emitting more Wattage as photons rather than heat for equal Wattage inlet. The following experiment shows the degradation of CBZ over  $\text{TiO}_2\text{-Ni}$  under irradiation of 405 nm LEDs. For comparison, Figure 16 shows the results of a similar experiment using 365 nm LEDs.





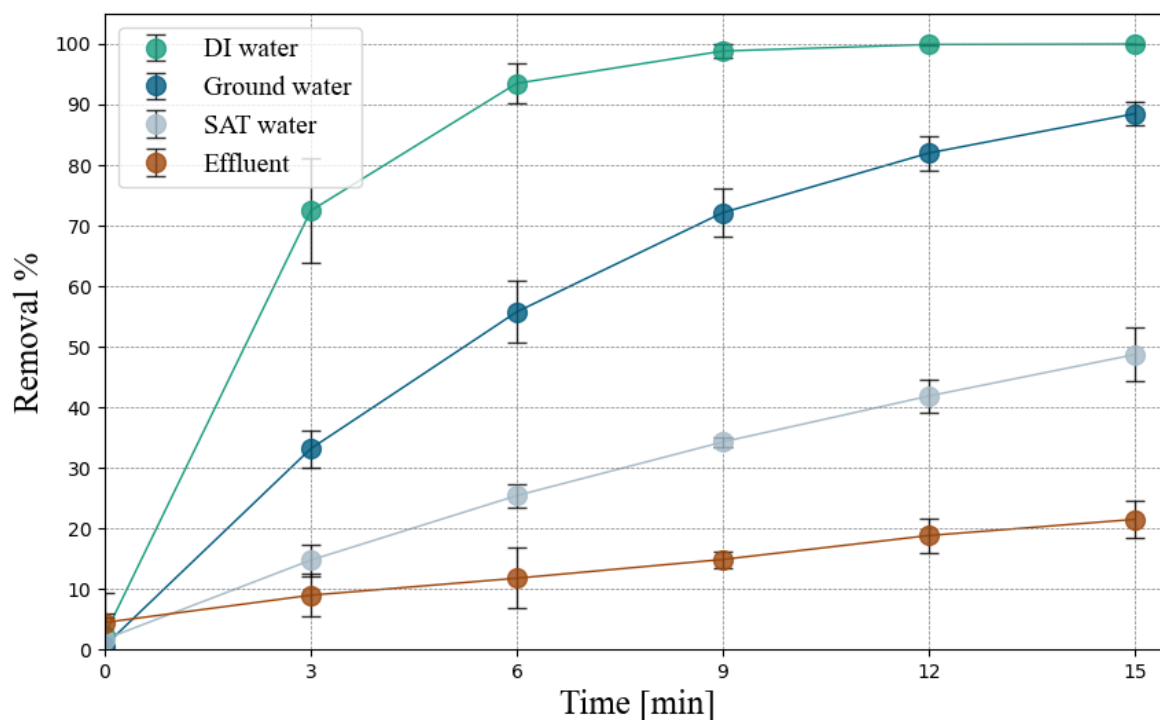
*Figure 16: CBZ removal under 365 nm LEDs (Blue) and 405 nm LEDs (green).*

The results presented in Figure 16 show a complete advantage for 365 nm LEDs over 405 nm LEDs, despite similar conditions, including wattage input. Moreover, higher wattage output in terms of light energy. The first conclusion that comes to one's mind, especially when knowing that LEDs are the main consumer of electricity, is that projecting photons of shorter wavelengths is preferable both in terms of degradation and energetic efficiency. However,  $\text{TiO}_2$  is known to have a band gap of 3-3.2 eV (mostly depending on its phase) that demands photons of 345-365 nm in wavelength, and therefore inferior results with 405 nm LEDs are expected. To utilize the advantage of better efficiency of 405 nm LEDs, other catalysts are required. Nowadays, most commercial photocatalysts are the ceramic type of oxide transition metals (Ti, Zn, Cu, etc.), with a wide band gap and, therefore, can not be sufficiently activated by wavelengths of  $\sim 400$  nm. The advancement in the development of photocatalysts efficient under wavelengths  $>400$  would be a significant leap forward.

## **2.6. Water matrices**

The developed technology described here is specified as a complementary treatment method for existing technologies. During the water recycling process, there are several stages; after each one, the water is unloaded of another pollutant. Some anthropogenic OMPs persist even after biological treatment (secondary treatment) and chlorination or SAT (soil aquifer treatment). The degradation of CBZ was tested in a few different water matrices: DI, effluents (secondary water post 50  $\mu\text{m}$  filtration), groundwater, and SAT water. The conditions in the

experiments described are 0.5 L of treated water with 1 ppm CBZ and a flow rate of 40 LPH. Details regarding water The results are in Figure 17.



*Figure 17: CBZ removal in different water matrices.*

DI water matrix provides the best conditions for removal, with no presence of organic material, the highest possible UV transmittance, and other components (divalent ions  $\text{Ca}^{+2}$ ,  $\text{Mg}^{+2}$ , metal ions, alkaline  $\text{-HCO}_3$ , etc.) that can change the removal rate, for good or bad. The removal results show 100% removal in 9 minutes. Moreover, since the goal is 80% removal, ~4 minutes are sufficient for that end.

The results show that the removal of CBZ in the effluent water matrix is the lowest of all four tested water matrices, reaching ~20% removal within 15 minutes. The low CBZ removal is mainly attributed to both the turbidity and organic content (TOC). The effluent water received from Shafdan measured a turbidity value of 1.7 NTU, a TSS value of  $4.4 \text{ mg L}^{-1}$ , and light transmittance ranges from 80% to 90% (in wavelengths in the range of 200-400 nm, see Figure 18). The direct impact of these values is in the utilization of projected photons, which are absorbed into the water or scattered rather than reaching and activating the photocatalyst. In order to compensate for the loss of photons, the power of LEDs could be increased, which will produce more photons. However, this action contradicts the primary goal of reducing the cost of operation and emission of GHGs. It is worth noting that samples from the same point reached a turbidity value of 3.9 NTU and a TSS value of  $7.4 \text{ mg L}^{-1}$  in the same month of sampling the water used for this experiment. This point is essential since it poses a greater

challenge for photocatalysis. Another cause of inferior degradation is the high concentration of total organic carbon (denoted as TOC) with a value of  $10.6 \text{ mg L}^{-1}$ , from which  $9.9 \text{ mg L}^{-1}$  is dissolved organic carbon (DOC), vs.  $1 \text{ mg L}^{-1}$  CBZ. DOC is an organic compound much like CBZ and other OMPs and, therefore, acts as a radical scavenger that reacts with ROSs produced by the photocatalytic process. This is a competing reaction to that of CBZ, with the advantage of quantity. The assumption is that out of the two causes, the high DOC value is the leading cause of low photocatalytic activity, mainly due to the fact that relatively high light transmittance allows a high portion of photon transmittance (see Figure 18) towards the photocatalyst. However, the high content of TOC/DOC scavenges the photoinduced ROSs.

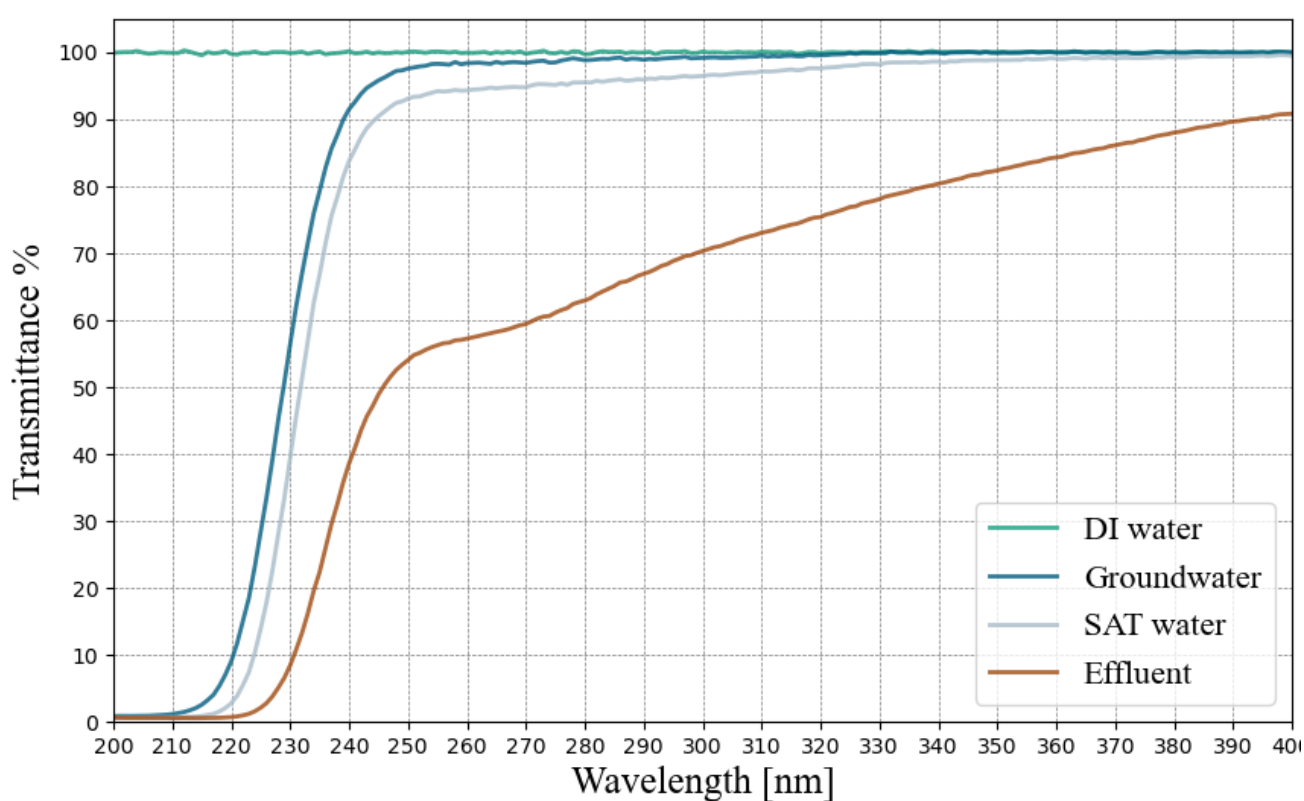


Figure 18: UV transmittance of varying water matrices in the range of 200-400 nm.

CBZ removal in the groundwater and SAT water matrices shows deterioration compared to DI water but superior removal compared to effluent water. There is a notable removal gap in favor of the groundwater, 49% vs. 89%, respectively. The SAT water has a turbidity of 0.4 NTU, not in the range of 1.7 or higher NTU of the effluent water matrix and closer to that of DI water and groundwater (0.1 NTU). However, unlike DI and groundwater, SAT water has a DOC content of  $0.8 \text{ mg L}^{-1}$ , close to  $1 \text{ mg L}^{-1}$  CBZ. In accordance with the effluent results, the presence of DOC has an impact on the total removal of CBZ.

Table 3: Water matrices contamination content.

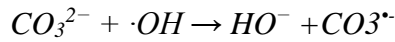
	DI	Groundwater	SAT	Effluent
DOC [mg L <sup>-1</sup> ]	0	0	0.8	9.9
TOC [mg L <sup>-1</sup> ]	0	0	N/A	10.6
TSS [mg L <sup>-1</sup> ]	0	0	N/A	4.4-7.4
Turbidity (NTU)	0.1	0.1	0.4	1.7-3.9

### 2.6.1. Chemical composition and pH effect on photocatalytic activity

Apart from DOC, natural water matrices, groundwater, SAT, and effluent water also contain divalent ions, Ca<sup>2+</sup> and Mg<sup>2+</sup> (the main sources of water hardness), sodium, free chlorine, etc. Moreover, pH also varies in these water matrices, and, as was demonstrated in the 2022 report (see Figure 19), has an impact on the degradation of OMPs, and CBZ among them.

The attraction-repulsion forces between the catalytic surface, reactants, and pollutants are partially dictated by the pH of the solution, making the pH a vital parameter<sup>14</sup>. Although CBZ is a neutral molecule in a wide range of pH values, and the photocatalytic surfaces' zeta potential values are similarly negative (Figure 10), the photocatalytic degradation results differ under varying pH values.

The impact of various components was demonstrated by Selvam et al.<sup>15</sup>, who reported a beneficial effect of transition metal ions on the degradation of 4-fluorophenol following the order: Mg<sup>2+</sup> > Fe<sup>3+</sup> > Fe<sup>2+</sup> > Cu<sup>2+</sup>, and an inhibitory effect of inorganic anions on the degradation of 4-fluorophenol following the order: CO<sub>3</sub><sup>2-</sup> > HCO<sub>3</sub><sup>-</sup> > Cl<sup>-</sup> > NO<sub>3</sub><sup>-</sup> > SO<sub>4</sub><sup>2-</sup>. Specifically, CO<sub>3</sub><sup>2-</sup> and HCO<sub>3</sub><sup>-</sup> are presented in the water matrices as alkalinity as HCO<sub>3</sub><sup>-</sup>, ranging in concentration of 170-230 mg L<sup>-1</sup>, and are known to scavenge ·OH radicles<sup>16,17</sup>, described by Equations 10 and 11.



(11)

Chlorine ions are also capable of reacting directly with the hole in the valence band of the catalyst, producing chlorine radicles<sup>18</sup>.

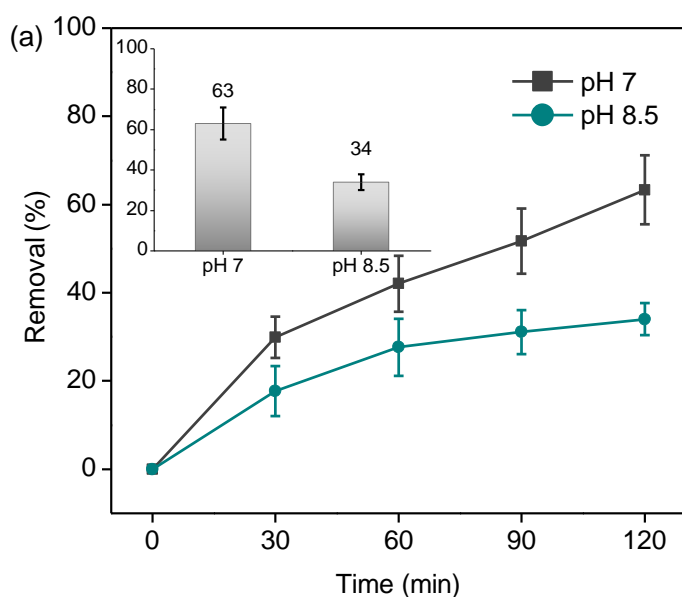


Figure 19: CBZ removal in lab scale reactor under varying pH values.

From the perspective of application development, the important point is that the water pH and chemical content are given, and any manipulation that can be done in a lab or pilot scale is not likely to be applied to large scales of water. pH adjustment, for example, requires adding other chemicals to the water, which is not desired. Moreover, despite any literature survey or experiment conducted, natural water matrices, effluents, SAT, or groundwater are composed of multiple chemical components at varying concentrations and pH in every sample. Therefore, it is impossible to predict the impact of each component due to the possible effect of components on each other.

Another aspect regards CBZ, which was used as a target pollutant mainly because it was vastly investigated. Apart from CBZ, many other pollutants are present in water matrices; each one is affected differently by the water conditions, operational parameters, etc.

### 3. Conclusions

Commercial TiO<sub>2</sub> powder coating over Ni foam via the EPD method was demonstrated in previous years. It has now been successfully upscaled from dimensions of 9.2 cm<sup>2</sup> (lab reactor) to 441 cm<sup>2</sup> (pilot scale). The pilot-scale reactor was used to examine the degradation of organic micropollutants using CBZ as a target pollutant from the upscaled reactor. Characterization of TiO<sub>2</sub>-Ni showed a uniform TiO<sub>2</sub> layer covering both the inner pores and outer layers of the 3D Ni foam without compromising the catalyst's phase or activity. Under optimized conditions, the TiO<sub>2</sub>-Ni catalyst exhibited 80% degradation of CBZ (1 mg L<sup>-1</sup>) within 4 minutes of total experimental time. Retention time and actual retention time calculations were made both for 1 and 0.02 ppm CBZ. The importance of physical parameters

was demonstrated with the catalyst and the wavelength of the emitted photons at wavelengths of 365, along with the impact of flow rate, which gave the best results at 40 LPH. 4 different water matrices were examined and showed that photocatalysis is limited in effluents. However, it can be applied to degrade organic micropollutants in ground and SAT water matrices. These findings highlight the potential of EPD combined with 3D metal foam substrates to create a 3D-coated PC reaction bed, showcasing its efficiency in removing emerging contaminants from water, with a potential for further scaling to a pilot level.

### **Fraunhofer Technical team**

#### **1. WP1: Definition of minimum treatment efficiency**

For the two applications a) WWTP effluent and b) water (surface or groundwater), the target quality parameters were summarized in a separate report based on German/European and Israeli legislation. For both applications, corridors with acceptable energy requirements were defined by comparison with the state-of-the-art (SOA) and the best available technology (BAT), namely ozone treatment and PAC (Powdered Activated Carbon).

#### **2. WP3: Test of System 1a with spiked effluent of Stuttgart Bösau WWTP.**

The most efficient catalyst coatings and operating conditions for the combination of titanium dioxide-coated nickel foams were determined by TAU in WP2. The coated membranes were integrated into a flow-through system with irradiation at a wavelength of 365 nm. This setup was sent by TAU to IGB. This “System 1a” was first tested with a methylene blue solution to compare its performance directly with established catalytic TiO<sub>2</sub> processes. Initial studies were conducted to evaluate the effects of volume flow and LED intensity on the degradation of methylene blue (MB). This was followed by further tests with spiked samples. In addition, reaction engineering investigations were carried out in WP3 on the existing test system 1a. Calculating reaction engineering metrics was essential for comparing different treatment methods and designing the reactor for scaling up. Key tools included actinometry, oxidation potential by free radicals (scavenging potential), and residence time distribution during pollutant degradation. These tools helped identify performance limitations and optimization potential.

Based on these findings, alternative materials and coatings were tested to support TAU in WP4. A new reactor system, designed for visible light and potential sunlight operation, was built. Catalysts from the literature were prepared at IGB and applied to both the nickel foam

carrier and a 3D-printed structure using various methods. In addition to dye degradation tests, reaction engineering investigations on actinometry and residence time distribution were performed similarly to test system 1a. Due to the reactor's open-atmosphere design, the measurement of oxygen-sensitive OH radicals could not yet be conducted. The results from WP3 were discussed in detail with TAU and fed into the planning and construction of the pilot plant in Israel (WP5). While TAU managed the implementation and operation on site, IGB used the additional experiments to further evaluate the performance of the developed reactor system in an impartial, technology-independent manner and identified areas for further optimization.

### **Summary of the experiments/investigations carried out in WP3:**

1. Volume flow influence and LED intensity influence on MB degradation rates in a Ni foam-based PCR (System 1a)
2. Degradation tests with iodinated contrast media in water spiked with effluent (System 1a)
3. External photonic efficiency by ferrioxalate actinometry (System 1a)
4. Scavenging potential determination with pCBA (System 1a)
5. Analysis of the residence time distribution (System 1a)
6. Identification of performance limitations and possibilities for optimization (System 1a)
7. Development of an advanced solar-based reactor concept
8. Evaluation of different solar catalysts
9. External photonic efficiency and residence time distribution in the solar reactor

#### **2.1. Volume flow influence and LED intensity influence on MB degradation rates in a Ni foam-based PCR (System 1a)**

Methylene Blue (MB) was used as a benchmark substance. To prepare the MB (Merck, 1.59270.0100) stock solution, 40 grams of MB were dissolved and diluted to a final volume of 4 liters with MilliQ water (provided by the MembraPure system), resulting in a stock concentration of 1000  $\mu\text{mol/l}$ . For the working solution with a concentration of 10  $\mu\text{mol/l}$ , the stock solution was diluted 1:100. Experiments were carried out using  $\text{TiO}_2$ -coated nickel foam ( $\phi = 95.2\%$ ) under various flow and irradiation conditions. The objective of these experiments was to evaluate the performance of nickel foam as a carrier material for  $\text{TiO}_2$  nanoparticles in a lab-scale photoreactor and to establish useful correlations between different parameters.

Volume flow influence: Benchmark degradation of MB in MilliQ water on the Ni foam catalyst reached degradation rates up to 6.6 nM/s with a corresponding flow rate of 0.28 l/h (see Figure 20). The highest long-term degradation rate was 6.3 nM/s, meaning that related

to the mean residence time ( $\theta = 4.7$  min), the change of the absolute concentration is the highest. Whereas for a comparably small volume flow of 0.025 l/h and hence the longest residence time of 53.2 min tested, the degradation rate dropped by 75 % to the lowest measured value of 1.6 nM/s. Interestingly, operating the system at 0.07 l/h and a residence time of 20.1 min showed a higher degradation rate in both conducted runs compared to the concentration changes by operation at 0.15 l/h with a mean irradiation time of 9.6 min.

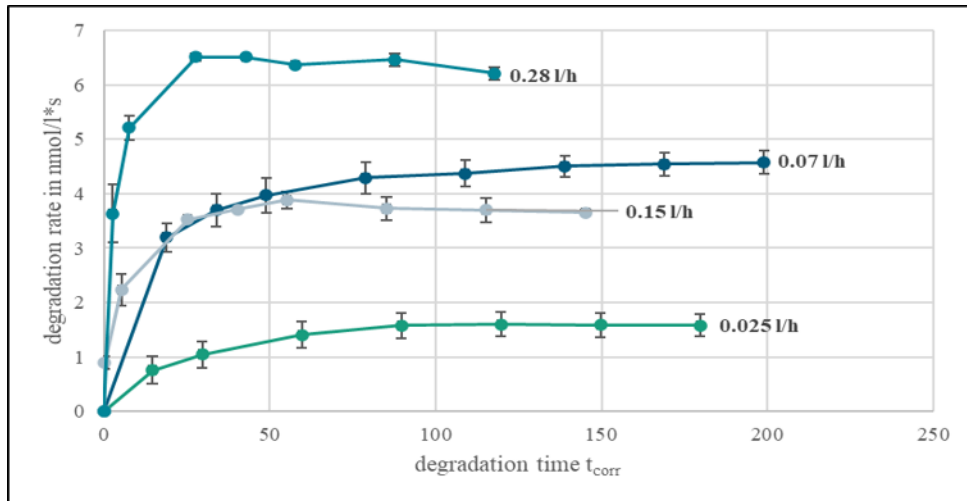


Figure 20: Degradation rates of MB using different volume flows in system 1a with a  $TiO_2$  Ni foam membrane.

The degradation rate values are calculated based on the mean residence time an MB molecule spends in the irradiated reactor volume at a certain flow rate. Therefore, it is also a measure of efficiency by referring to the change of concentration over time to the associated residence time. In addition to the degradation rate, the total removal value states a very important experiment-specific figure of merit, the decision on which volume flow is the most effective needs to be made based on both values. Therefore, operating the system at 0.07 l/h is the most effective volume flow since it shows the second highest degradation rate of 4.5 nM/s and a way higher total removal value of 54 % compared to the total removal of 17 % at 0.28 l/h. Even if running the system at 0.28 l/h leads to a higher throughput of 1 l during 200 min operation time, the quite low total removal of 17 % is a great disadvantage. In comparison, treatment of 230 ml at 0.07 l/h results in a significantly higher total removal of 54 %. For these reasons, the volume flow of 0.07 l/h was used for further parameter experiments.

LED intensity: Since all runs for the determination of the influence of the LED intensity on MB degradation were performed at 0.07 l/h, the different results are only based on different LED intensities. Results of the graphs for different irradiation intensities (see Figure 21) show saturation curve characteristics with a plateau concentration. The highest steady-state



degradation rate of 4.5 nM/s is obtained at the highest irradiation intensity of 25 mW/cm<sup>2</sup>. The medium setting of 16.3 mW/cm<sup>2</sup> did reach a steady state degradation rate of 3.3 nM/s, whereas the lowest irradiation intensity of 8 mW/cm<sup>2</sup> reached a value of 2.6 nM/s. In terms of relative deviation, the average of runs with 25 mW/cm<sup>2</sup> has a 36 % higher degradation rate than the average of runs with 16.3 mW/cm<sup>2</sup> and a 42 % higher degradation rate than the average of runs with 8 mW/cm<sup>2</sup>.

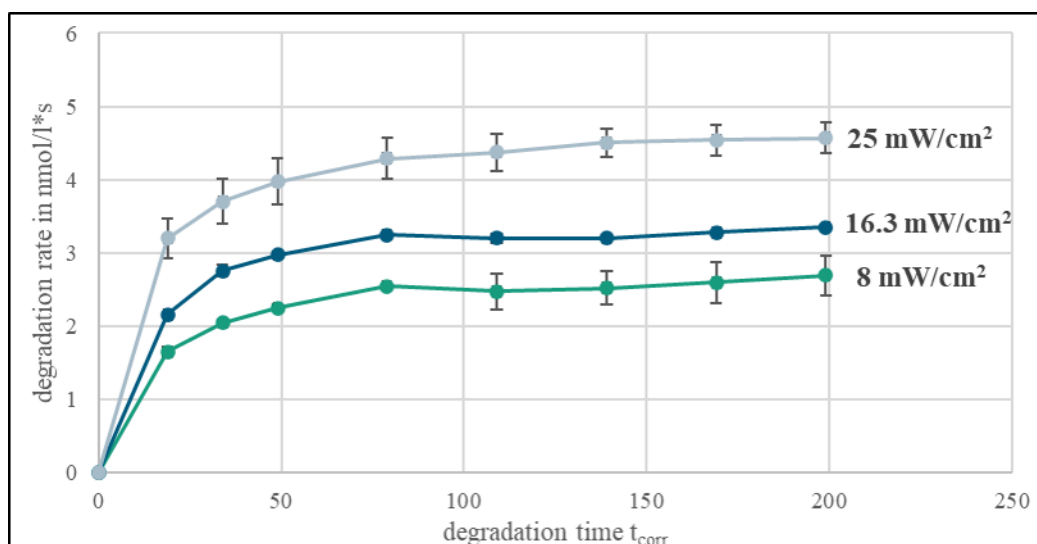


Figure 21: Degradation rates of MB using different irradiation intensities in system 1a with a TiO<sub>2</sub> Ni foam membrane.

As expected, a trend of increasing degradation rate with increasing irradiation intensity was confirmed. Therefore, the enhanced irradiation intensity did increase the photocatalytic reaction rate in the reactor by providing more photons. Since 25 mW/cm<sup>2</sup> is the highest possible LED setting, there is a possibility that the degradation rate can be further increased until reaching other limitations than photon limitation at a certain point. At this point, a further increase in the irradiation intensity and, therefore, the number of photons would not increase the degradation rate because every available active site of the photocatalyst would already participate in the reactions. Additionally, it was shown that the Ni foam showed no decrease in performance over time due to MB adsorption.

## **2.2. Degradation tests with iodinated contrast media in water spiked with effluent (System 1)**

Iodinated contrast media are emerging contaminants. The iodinated X-ray contrast media (ICM) Iohexoland and Iopamidol were tested to determine how efficiently their concentrations can be reduced by photocatalytic treatment. Three different water matrices were used. The matrices applied are distilled water (DW), tap water (TW) and actual

wastewater treatment effluent after the third treatment step (WW) from the local treatment plant in Bösau in Stuttgart, Germany. Additionally, all three matrices were tested with two different irradiation intensities (11 mW/cm<sup>2</sup> and 26 mW/cm<sup>2</sup>) and three different irradiation times (21.4 min, 8.5 min and 3.2 min). The ICM Iohexol and Iopamidol in different water matrices revealed lower degradation rates for increasing water matrix complexity, ranging from 0.45 nM/s to 0.05 nM/s (see Figure 22 and Figure 23).

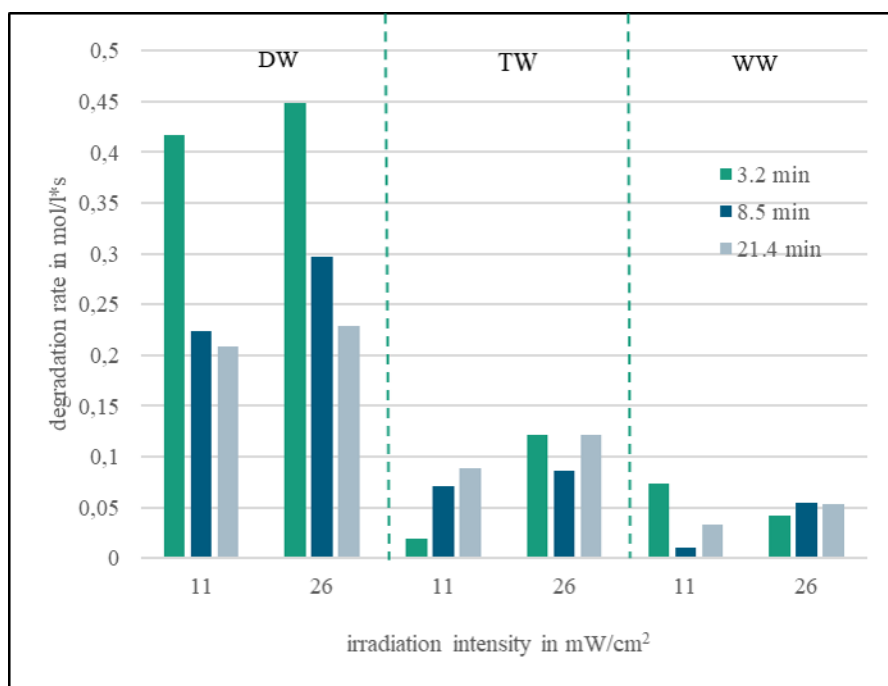


Figure 22: Degradation rate of Iohexol with different water matrices, irradiation intensities and times.

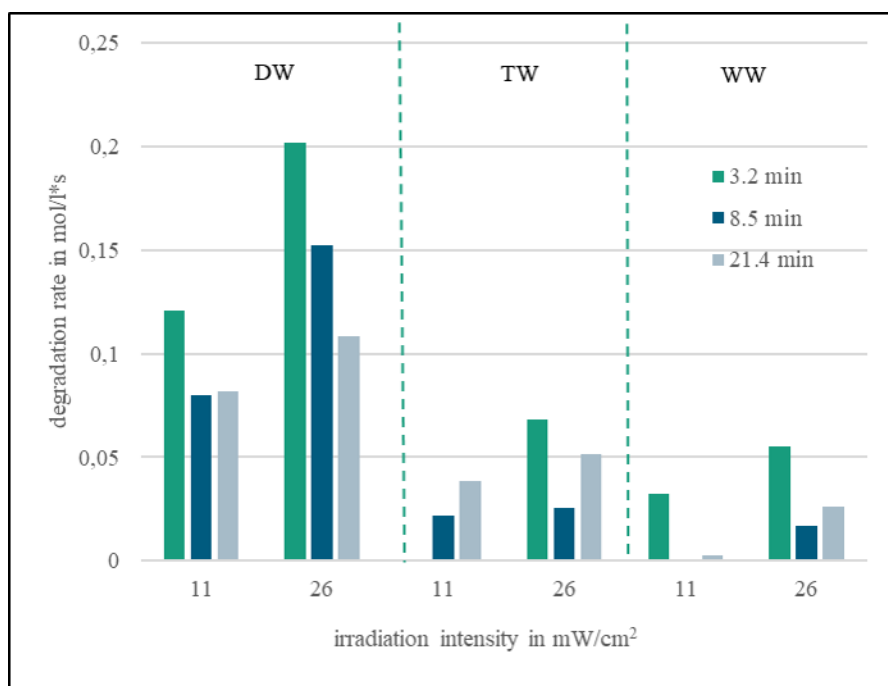


Figure 23: Degradation rate of Iopamidol with different matrices, irradiation intensities and times.

Further results show that Iohexol is significantly easier to remove by photocatalysis than Iopamidol (relative difference of >55 % in DW with 3.2 min residence time and 26 mW/cm<sup>2</sup>).

### 2.3. External photonic efficiency by ferrioxalate actinometry (System 1a)

Actinometry experiments show an overall external photonic efficiency of 15.7 % for the lab-scale setup (see Figure 24). This value is key for the subsequent scale-up, and specific design rules, such as a design basis to evaluate the geometrical overlap of the irradiated area and the photocatalyst-coated Ni-foam surface, have been established.

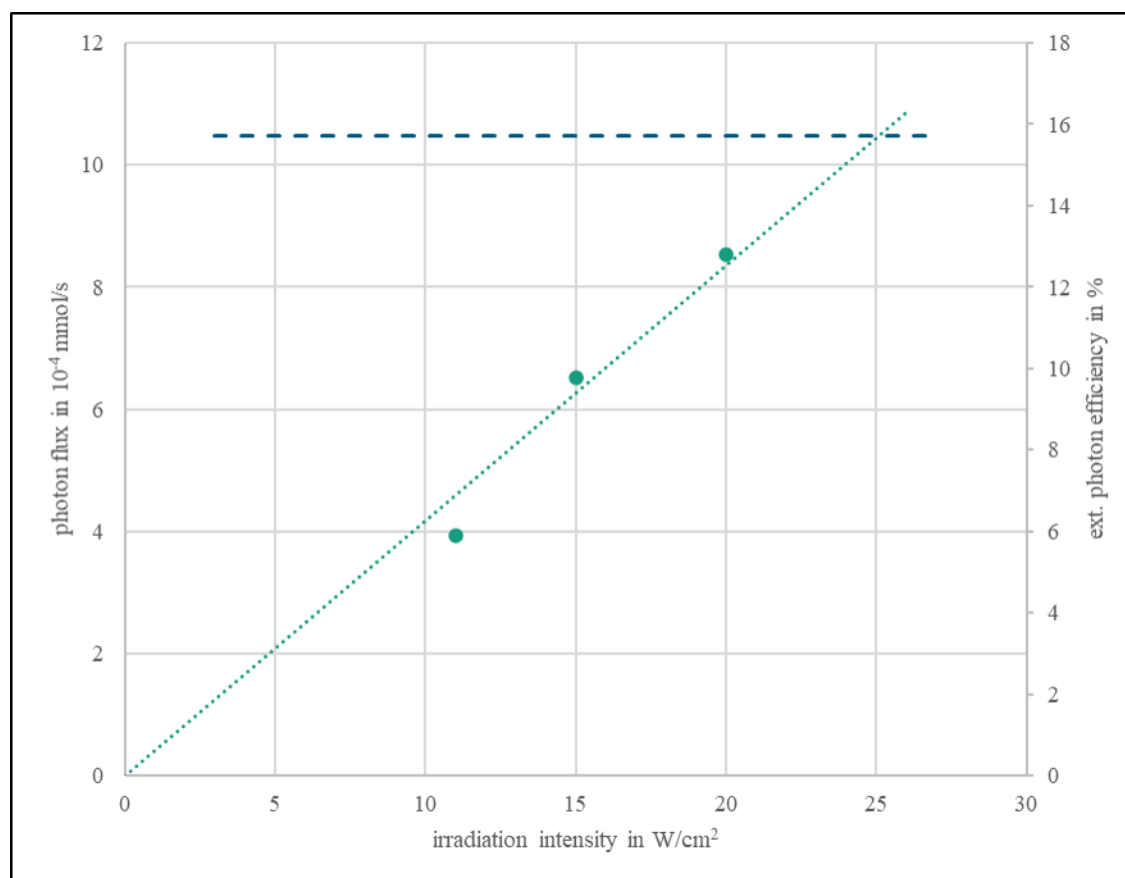


Figure 24: Experimentally determined available photon fluxes and external photonic efficiencies by ferrioxalate actinometry of system 1a.

### 2.4. Scavenging potential determination with pCBA (system 1a)

In order to characterize the scavenging potential of the catalytic membrane reactor, a method for photometric quantification of the OH radicals was adapted to the intensified conditions in the applied reactor setup. This is done using the indicator substance para-chlorobenzoic acid (pCBA). Usually monitored by time-delayed HPLC-MS/MS, the method has been modified to give both in-situ data using UV/Vis spectroscopy for continuous concentration

determination with a flow-through measuring cell and providing data in a regularly taken sample that can immediately be measured in a UV/Vis spectrometer. The lowest OH radical formation rates are measured at the lowest volume flow (see Figure 25). When measured with the photometer, this is  $0.3 \text{ nmol s}^{-1}$  at  $0.53 \text{ mL min}^{-1}$ . With an increasing

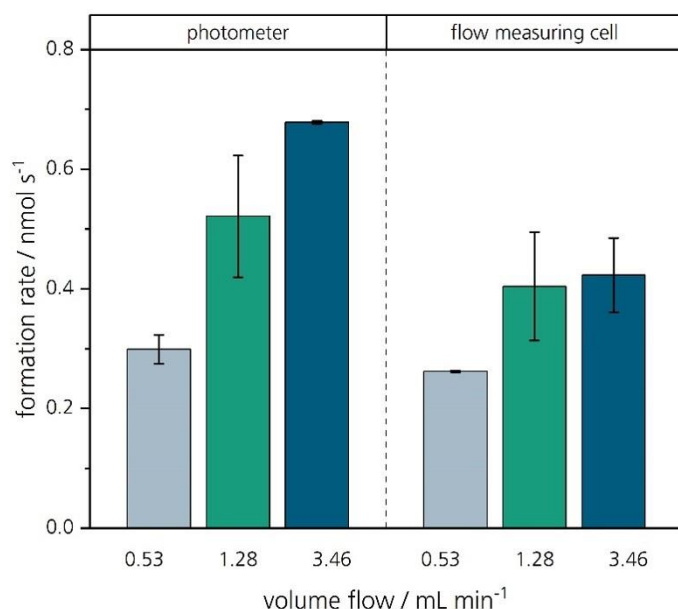


Figure 25: Formation rate of OH radicals dependent on the volume flow, measured in both the photometer and the flow cell of system 1a.

With a volume flow of  $3.46 \text{ mL min}^{-1}$ , the degradation rate increases by around 42 % to  $0.7 \text{ nmol s}^{-1}$ . The dependence of the formation rate from the volume flow was as expected since it can be attributed to the diffusion limitation in the reactor and the formation of short-circuit flows and dead zones.

## 2.5. Analysis of the residence time distribution (System 1a)

The measurement of the residence time distribution in the reactor shows the formation of shortcuts and dead zones, especially at low-volume flows. The mean actual residence time deviates up to 48 % from the hydrodynamic residence time. This flow behavior leads to reduced efficiency of the degradation and the usable amount of catalyst surface available per time interval. The discussion in comparison to the developed solar reactor model can be found in i

## 2.6. Identification of performance limitations and possibilities for optimization (System 1a)

By establishing tools to measure the radicals generated, a comprehensive, process-step-resolved perspective of the limiting factors can be achieved. To visualize the main influences on the efficiency and constraints of the reactor design, a Sankey diagram of the various

pollutant degradation reaction steps was developed (see Figure 26).

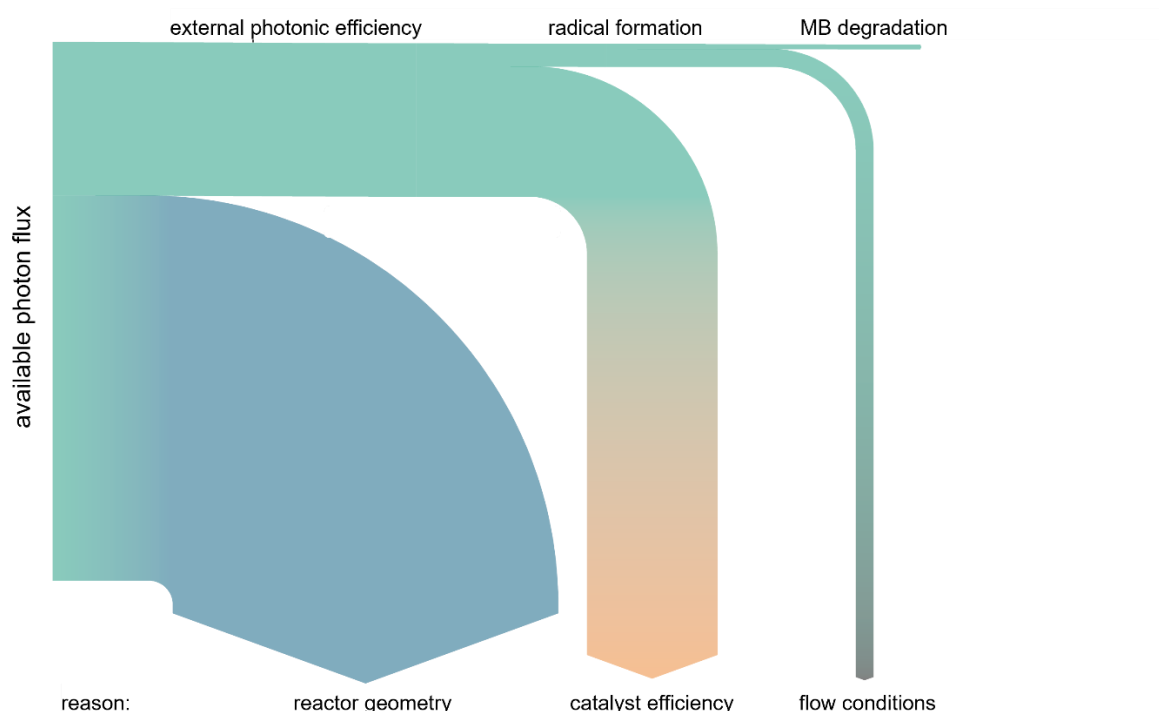


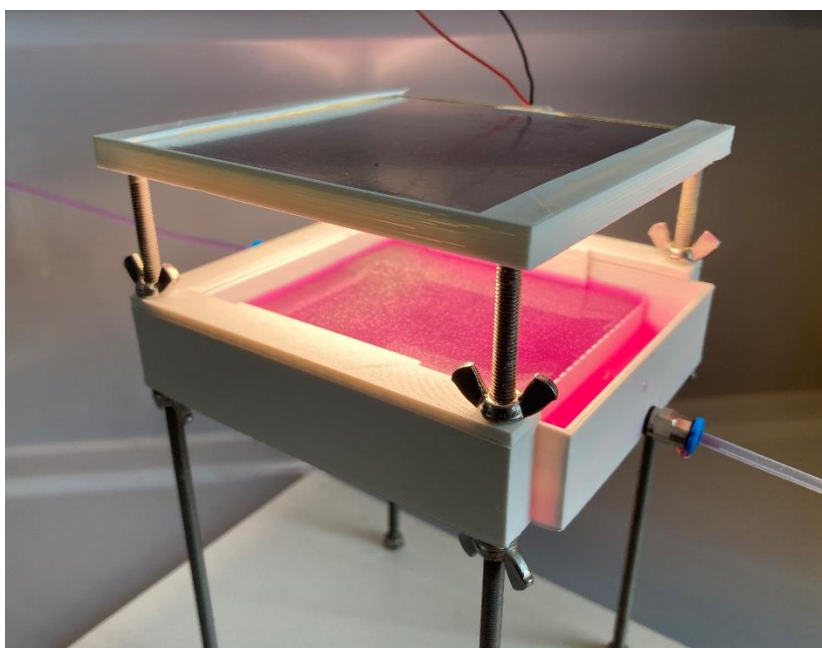
Figure 26: Sankey diagram of the photon flux available in the reactor volume of system 1a.

It can be clearly seen that most of the efficiency is already lost when the emitted photon flux of  $1.19 \mu\text{mol s}^{-1}$  hits the reactor surface. Only approximately 29 %, or  $0.34 \mu\text{mol s}^{-1}$ , reach the reaction chamber through the irradiation window. The other 71 % hit the edge of the reactor or suffer from reflection and scattering and, therefore, cannot react with the catalyst. The photon flux that enters the reactor and reaches the catalyst, in theory, generates hydroxyl radicals. The method developed can be used to measure radicals that are generated and react with the pCBA (about  $0.5 \text{ nmol s}^{-1}$ ). However, there are also considerable losses of up to 20 % due to other reaction pathways like simple deactivation or energy transfer to the solvent. Accordingly, the ratio of formation is less than 1% of the original photon flux that is theoretically available in the reactor. A main finding from this is that the quality of the coating of the catalyst carrier and, thus, the amount of catalyst available can be significantly improved to optimize the radical formation rate.

## 2.7. Development of an advanced solar-based reactor concept

This work package focuses on transforming the gained insights towards photocatalysis initiated by visible light, which is promising to be more energy-efficient than traditional UV-based photocatalysis since the photons, in theory, carry about only half the energy but cause

the same catalytic effect. In situations where direct sunlight is not available or as reliable irradiation support, OLEDs (Organic Light-Emitting Diodes) offer a suitable solution. They, therefore, might enable an even more efficient and sustainable water treatment. For this purpose, a new reactor geometry was designed to investigate photocatalytic wastewater treatment using an OLED. The reactor model was aligned with a selected OLED and is based on the principle of flow through. In contrast to the catalytic membrane reactor, the reactor was designed openly, with a large intake and an exit edge for outflow. Realization of the model was via 3D printing.



*Figure 27: 3D printed solar reactor.*

## **2.8. Evaluation of different solar catalysts**

Three different catalysts were selected for the photocatalytic investigations under visible light: titanium dioxide (KronoClean 7000), bismuth tungstate, and graphitic carbon nitride. All of them can be used variably in the developed reactors. As a catalyst support, the catalysts were either coated on 3D-printed PLA material using a geopolymer-based coating (potassium silicate and a calcium aluminate-based hardener, 5.7 wt.% catalyst) or immobilized on the nickel foam with electrophoretic deposition (EPD). Figure 28 shows the differently coated supports.


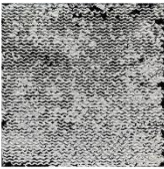


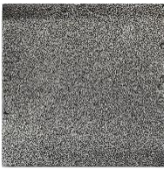
<i>catalyst</i> <i>support material</i>	<b>KRONOClean ® 7000 (TiO<sub>2</sub>)</b>	<b>Bismuth tungstate (Bi<sub>2</sub>WO<sub>6</sub>)</b>	<b>Graphitic carbon nitride (g-C<sub>3</sub>N<sub>4</sub>)</b>
<b>3D PLA print</b>			
<b>Nickel foam</b>	—		

Figure 28: Scheme of the investigated combinations of catalysts and catalyst supports.

Batch tests were carried out to test the catalysts for photocatalytic activity. The catalysts were immersed in cationic (methylene blue, MB) and anionic (rose bengal, RB) dyes for 1 h and tested under different light conditions. High MB adsorption on the immobilized geopolymer catalyst was observed, while no significant RB adsorption was noticed. Under OLED irradiation, the catalyst geopolymer coating showed differences compared to the dark sample, while a clear difference was observed under UV irradiation.

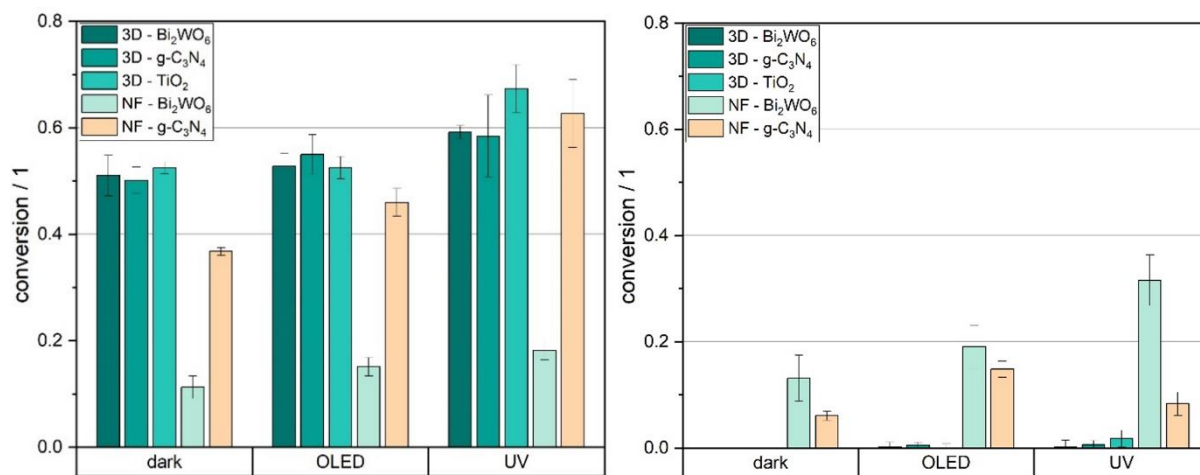


Figure 29: Degradation of methylene blue (left) and rose bengal (right) from different catalysts and irradiation.

The two nickel foams coated with catalyst showed interactions with both dyes. Despite the small amount of bismuth tungstate that could be immobilized on the foam, photocatalytic activity was observed under OLED and UV irradiation. The graphitic carbon nitride (CN) showed similar adsorption of MB as the geopolymer coatings and a photocatalytic effect when exposed to visible and UV light. Under UV conditions, the graphitic carbon nitride shows a

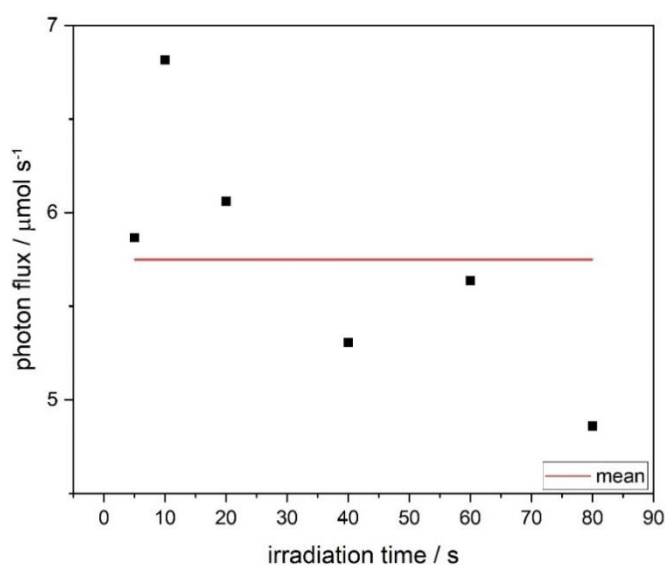
lower conversion for RB, which needs further investigation to conclude a meaningful explanation.

The strong adsorption effects on the geopolymer coating and CN can be attributed to its chemical and physical properties that lead to a net negative charge and allow preferential binding of the cationic MB.

Testing real target pollutant degradation in continuous experiments, the pharmaceutical component carbamazepine was investigated on its photocatalytic degradation. The various immobilized catalysts were examined in the developed flow-through reactor under OLED irradiation. It was found that none of the catalysts caused adsorption or degradation of this component, though. Investigations on the reason for the failed proof of concept are underway.

## **2.9. Actinometry and residence time distribution in the solar reactor**

The actinometric experiments in the solar reactor quantified the available photon flux in the reactor volume to a comparably high rate of  $5.76 \mu\text{mol s}^{-1}$ . (see Figure 30) The external photonic efficiency was determined to be 93.3%, which indicates a very efficient use of light. These results confirm the very suitable design of the reactor geometry for the light source. The residence time distribution is one variable used to assess the flow conditions within the reactor. The sum function  $F(\theta)$  of the residence time describes the cumulative probability distribution of the time that a fluid element remains in a system before leaving.  $F(\theta)$  is usually plotted over the dimensionless time  $\theta$ , which is the actual residence time normalized by the hydrodynamic residence time. The monitoring of mixing in a reactor is of crucial importance for the characterization of flow processes.



*Figure 30: Actinometry results in the solar reactor*



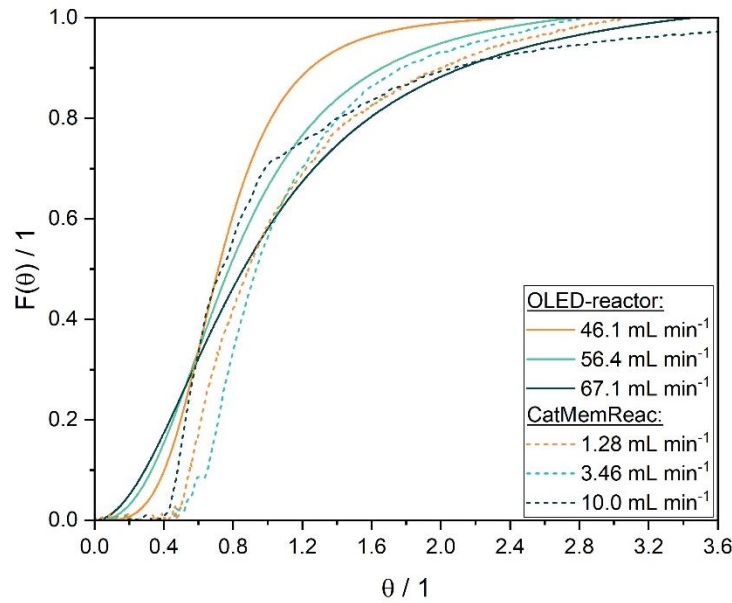


Figure 31: Residence time distribution function of the solar reactor vs. the CatMemReac (System 1a) concept.

A significant difference is that the curves of the catalytic membrane reactor start rising later than those of the OLED reactor (see Figure 31). The slope of the CatMemReac curves corresponds approximately to the lowest volume flow of the OLED reactor. In general, the curves of the OLED reactor show a more homogeneous distribution. The flow conditions in the OLED reactor are better, especially at the beginning of the mixing time. It should, therefore, be noted that a larger volume flow should be aimed in order to achieve effective mixing and distribution. No long-lasting dead zones in the OLED reactor were observed, which indicates a positive design of the reactor systems. In addition, the hydrodynamic and exact residence time values, as well as the Bodenstein number and the (theoretical) vessel count, can be compared between the two different reactors.

Table 4: Different calculated values from the residence time distribution of the solar reactor

<b>Volum e flow</b> $\dot{V} / \text{mL min}^{-2}$	<b>Hydrodynam ic residence time</b> $\tau / \text{s}$	<b>Actual residence time</b> $\bar{t} / \text{s}$	<b>Bodenstei n number</b> $Bo / 1$	<b>(theoretical ) Vessel count</b> $N / 1$
<b>46,1</b>	247,5	193,5	21	11
<b>56,4</b>	202,2	181,0	16	8

67,1	169,8	177,6	14	7
------	-------	-------	----	---

*Table 5: Different calculated values from the residence time distribution of the System 1a*

<b>Volum e flow</b> $\dot{V} / \text{mL}$ $\text{min}^{-2}$	<b>Hydrodynami c residence time</b> $\tau / \text{s}$	<b>Actual residenc e time</b> $\bar{t} / \text{s}$	<b>Bodenstei n number</b> $\text{Bo} / 1$	<b>(theoretical ) Vessel count</b> $N / 1$
<b>1,28</b>	18,34	11,28	38	19
<b>3,46</b>	6,78	4,83	31	16
<b>10,00</b>	2,35	1,21	18	9

The Bodenstein number  $\text{Bo}$  describes the ratio of convective mass transfer and axial mixing in the reactor. The degree of backmixing decreases as the Bodenstein number increases. The vessel count  $N$  describes a parameter of the cascade model. It indicates how many vessels are required to achieve complete backmixing. The Bodenstein numbers are all in the range that corresponds to a real stirred tank reactor. As the volume flow increases, both the Bodenstein number and the vessel count decrease. The observation of a lower Bodenstein number at higher volume flows indicates that the dispersion increases with increasing velocity. This can be explained by the increased mixing at higher volume flows.

## **LCA – TAU and Fraunhofer ISI**

### **WP 7: Ecologic evaluation of test system**

#### **1. LCA of alternative technologies (Led by Fraunhofer ISI)**

Three technologies for the removal of trace organic compounds from sewage water are already applied in sewage plants and must hence be considered as alternative technologies for comparison:

- Ozonation
- Powdered activated carbon (PAC)
- Granular activated carbon (GAC)

All three technologies increase the demand for electricity, chemicals, and ancillary materials (oxygen for ozone generation, production and reactivation of activated carbon) in sewage

plants significantly. The choice of one of the three technologies and its environmental impact depends on the application site, particularly on the specific water properties. A higher concentration of DOC leads to a higher demand for ozone or activated carbon, connected to higher GHG emissions.

Most of the available LCA studies on these technologies focus on primary energy demand and GHG emissions. There is little to no information about other impact categories (e.g., acidification, human toxicity, ecotoxicity). A particular challenge is that no impact models are available for the trace substances in focus, i.e., the environmental benefits of removing these trace substances cannot be considered in LCA studies. The infrastructure (reactors, etc.) has minor impacts on overall energy demand and GHG emissions; most important are the operating materials and the electricity demand. Therefore, the local electricity mix has a high impact on the overall GHG emissions (especially for ozonation).

The relevance of DOC removal by ozonation or activated carbon for the overall energy demand and GHG emissions of a wastewater treatment plant varies between 4 - 20% in different studies. There is no clear ranking regarding energy demand/GHG emissions of the three technologies. However, ozonation and GAC are mostly found to have lower GHG emissions than PAC. The primary energy demand for activated carbon production is higher than the primary energy demand for the production of liquid oxygen (required for ozone production).

Overall, there is no proof of the ecological benefit of these technologies from a life-cycle perspective (i.e., on a global scale). The motivation for implementing these technologies is their environmental benefit on a local scale, i.e. the improved water quality (reduced toxicity values) of local water body. However, local water quality benefits could be outweighed by increases in indirect impacts from energy and resource demands (upstream production of energy, chemicals, ancillary materials).

### **1.1. LCA data for ozonation**

The electricity demand of ozonation is the major driver of its GHG emissions. Therefore, GHG emissions depend highly on the electricity generation or electricity mix. Other relevant factors are the specific ozone dose needed and whether the ozone is produced on-site or delivered. Another relevant factor is the feed gas for ozonation, for which air or oxygen can be used. For the latter, the production of liquid oxygen is necessary, giving rise to additional electricity demand. However, with a European electricity mix, there are no significant differences in GHG emissions between ozonation with pure oxygen vs. air as feed gas.

Table 6 gives an overview of different data sources. The input data (oxygen, ozone, electricity,

natural gas, primary energy demand) is well covered, but values differ between sources.

*Table 6: Inputs needed for ozonation according to different literature sources. (Plattform Verfahrenstechnik Mikroverunreinigungen; Risch et al. 2022<sup>19</sup>; Mousel et al. 2017<sup>20</sup>; Meier and Remy 2020<sup>21</sup>, Jekel and Ruhl 2016, Boer et al. 2022<sup>22</sup>)*

<b>Input Flow</b>	<b>Quantity</b>	<b>Specific unit [ / ]</b>
<i>Source: <a href="https://micropoll.ch/">https://micropoll.ch/</a></i>		
<i>Input 1: Oxygen</i>		
<i>electricity demand</i>	0,8	kWh/kg O <sub>2</sub>
<i>primary energy demand</i>	0,05	kWh/kg O <sub>2</sub>
<i>Input 2: ozone</i>	0,75	g O <sub>3</sub> / g DOC
<i>Input 2: ozone</i>	0,4 to 0,7	mg O <sub>3</sub> / mg DOC
<i>electricity demand</i>	10	kWh / kg O <sub>3</sub>
<i>electricity demand</i>	0,06	kWh / m <sup>3</sup> treated water
<i>natural gas demand</i>	0,8	kWh / kg O <sub>2</sub>
<i>primary energy demand</i>	0.05	kWh / kg O <sub>2</sub>
<i>Source: Risch et al. 2022</i>		
<i>Input 1: Oxygen</i>	8,8	g O <sub>2</sub> / g O <sub>3</sub>
<i>Input 2: ozone</i>	0,78	g O <sub>3</sub> / g DOC
<i>Input 2: ozone</i>	6,22	g O <sub>3</sub> / m <sup>3</sup> treated water
<i>auxiliary: DOC</i>	8	g DOC / m <sup>3</sup> treated water
<i>electricity demand</i>	0,12	kWh / m <sup>3</sup> treated water
<i>electricity demand</i>	0,09	kWh / m <sup>3</sup> treated water
<i>Source: Mousel et al. 2017</i>		
<i>electricity demand</i>	0,26	kWh / kg LOX
<i>electricity demand</i>	0,64	kWh / kg LOX
<i>primary energy demand</i>	0,39	kWh / (1000 kg * km)
<i>electricity demand</i>	0,03 to 0,12	kWh / m <sup>3</sup> treated water
<i>electricity demand</i>	0,12	kWh / m <sup>3</sup> treated water
<i>electricity demand</i>	0,1 to 0,2	kWh / m <sup>3</sup> treated water
<i>electricity demand</i>	0,035	kWh / m <sup>3</sup> treated water
<i>electricity demand</i>	0,04 to 0,09	kWh / m <sup>3</sup> treated water
<i>electricity demand</i>	0,045	kWh / m <sup>3</sup> treated water
<i>electricity demand</i>	0,05	kWh / m <sup>3</sup> treated water

<i>Source: Meier &amp; Remy 2020</i>		
<i>electricity demand</i>	12,5	kWh / kg O <sub>3</sub>
<i>electricity demand</i>	0,03	kWh / m <sup>3</sup> treated water
<i>Input 2: ozone</i>	0,41 / 0,48 / 0,55	g O <sub>3</sub> / g DOC
<i>Input 2: ozone</i>	1,9 / 3,4 / 2,7	g O <sub>3</sub> / m <sup>3</sup> treated water
<i>electricity demand</i>	0,06	kWh / m <sup>3</sup> treated water
<i>electricity demand</i>	0,021/0,026/0,049	kWh / m <sup>3</sup> treated water
<i>Source: Jekel et al. 2016</i>		
<i>Input 2: ozone</i>	0,4 / 0,7 / 1	g O <sub>3</sub> / g DOC
<i>auxiliary: DOC</i>	12,8 / 6,4	mg / l = g / m <sup>3</sup>
<i>Input 2: ozone</i>	0,54 / 0,27	kt / year
<i>Input 2: ozone</i>	0,89 / 0,44	kt / year
<i>Input 2: ozone</i>	1,18 / 0,59	kt / year
<i>electricity demand</i>	13	kWh / kg O <sub>3</sub>
<i>Input 1: Oxygen</i>	10	kg O <sub>2</sub> / kg O <sub>3</sub>
<i>Source: de Boer et al. 2022</i>		
<i>Input 2: ozone</i>	500 to 2000	mg O <sub>3</sub> / g TOC
<i>Input 2: ozone</i>	30 to 1600	mg O <sub>3</sub> / g DOC
<i>Input 2: ozone</i>	1 to 200	mg / l = g / m <sup>3</sup>
<i>auxiliary: DOC</i>	1,5 to 25	mg / l = g / m <sup>3</sup>
<i>auxiliary: COD</i>	12 to 1500	mg / l = g / m <sup>3</sup>
<i>auxiliary: TOC</i>	5 to 400	mg / l = g / m <sup>3</sup>

## **1.2. LCA data for activated Carbon**

The main contribution to energy demand and GHG emissions for the activated carbon process comes from the production of activated carbon. Minor, negligible contributions are caused by transport and on-site electricity demand. Granular activated carbon (GAC) processes cause less GHG emissions than powdered activated carbon (PAC) processes due to the use of reactivated carbon. Hence, the share of reactivated carbon is important for the environmental impacts. Besides, the use of activated carbon can increase the amount of sludge, especially for PAC in high dosages.

The overall GHG emissions of PAC are mainly driven by raw materials (hard coal, lignite). They can be reduced by 40% when using renewable raw materials (e.g., wood, coconut husk). The on-site electricity demand of PAC is low, mainly due to PAC insertion.

Since GAC is based on the use of reactivated carbon, its GHG emissions are mainly caused by the energy demand for the reactivation process, and to a lesser extent by the raw materials for activated carbon. The onsite electricity demand is low again and mainly due to additional filters.

Table 7 shows an overview of different data sources for activated carbon. The input data (steam, natural gas, primary energy demand, electricity demand, hard coal, lignite, coconut husk) is well covered, but values vary in the literature.

*Table 7: Inputs needed for activated carbon according to different literature (Mousel et al. 2017<sup>20</sup>; Jekel and Ruhl 2016; DWA-Arbeitsgruppe KA-8.6 2016; Boer et al. 2022<sup>22</sup>).*

<i>Input Flow</i>	<i>Quantity/ Amount</i>	<i>Specific unit [ / ]</i>
<i>Source: Mousel et al. 2017</i>		
<i>coal</i>	2	kg / kg AC
<i>Steam</i>	3	kg / kg AC
<i>primary energy demand</i>	3	kWh / kg AC
<i>natural gas</i>	4,9	m <sup>3</sup> / kg AC
<i>primary energy demand</i>	54,4	kWh / kg AC
<i>electricity demand</i>	0,02	kWh / kg AC
<i>primary energy demand</i>	0,4	kWh / kg AC
<i>primary energy demand, total</i>	57,9	kWh / kg AC
<i>coal</i>	3	kg / kg AC
<i>Steam</i>	12	kg / kg AC
<i>primary energy demand</i>	12,1	kWh / kg AC
<i>natural gas</i>	0,33	m <sup>3</sup> / kg AC
<i>electricity demand</i>	1,6	kWh / kg AC
<i>primary energy demand, total</i>	13,7	kWh / kg AC
<i>primary energy demand</i>	0,08	kWh / (1000 kg*km)
<i>Source: Jekel et al. 2016</i>		
<i>hard coal</i>	3	t / t AC
<i>Lignite</i>	5	t / t AC
<i>coconut husk</i>	10	t / t AC
<i>Steam</i>	12	t / t AC
<i>natural gas</i>	280	m <sup>3</sup> / t AC
<i>electricity demand</i>	1600	kWh / t AC

<i>Source: DWA 2016</i>		
<i>hard coal</i>	3,5 to 5	t / t AC
<i>Lignite</i>	5 to 6,5	t / t AC
<i>coconut husk</i>	10 to 13	t / t AC
<i>Steam</i>	3 to 4	t / t AC
<i>electricity demand</i>	150 to 400	kWh / t AC
<i>natural gas</i>	(auto thermal process)	
<i>Steam</i>	None	t / t AC
<i>electricity demand</i>	11 bis 335	kWh / t AC
<i>natural gas</i>	80 bis 190	m <sup>3</sup> / t AC
<i>Source: de Boer et al. 2022</i>		
<i>auxiliary: TSS</i>	3 to 6	mg / l
<i>auxiliary: DOC</i>	6 to 11	mg / l
<i>auxiliary: COD</i>	21 to 31	mg / l

### **1.3. Data for comparison with the CatMemReac technology**

For a comparison with the CatMemReac technology, we chose the publication of Jekel and Ruhl (2016) as a benchmark. According to their research, for a typical German wastewater treatment plant with a DOC concentration of 12.8 mg/l the following global warming potentials of different technologies were estimated:

- **Ozonation: 0,28 kg CO<sub>2</sub>eq/m<sup>3</sup>**, including production of liquid oxygen, electricity consumption, sand filtration, infrastructure, removal of phosphorus
- **PAC: 0,28 kg CO<sub>2</sub>eq/m<sup>3</sup>**, including production of activated carbon, electricity consumption, sand filtration, infrastructure, removal of phosphorus

This is in line with a recent publication reporting the global warming potential to be 0.3 kgCO<sub>2</sub>eq/m<sup>3</sup> for water reclamation (Maniakova et al., 2023<sup>23</sup>). The value of energy used in ozonation for pharmaceutical removal is reported to be 0.75 kWh/m<sup>3</sup> (Arzate et al., 2019<sup>24</sup>). The main energy-consuming component for ozone production is the ozonator, which produces the spark leading to the release of ozone (Munoz et al., 2009<sup>25</sup>). Other components contributing to the electricity use in ozone production include pumps and the ozone destructor.

## **2. LCA of CatMemReac technologies at a lab and pilot scales (Led by TAU)**

In this section, we describe the environmental evaluation method and results for the lab and pilot scale stages.



## **2.1. Methodology**

We adopted ISO standards (ISO 14040) to perform the life cycle assessment (LCA) of the CatMemReac technology. The standard provides the following steps in a framework to calculate the environmental impacts of a product system.

### **2.1.1. Definition of the Goal and Scope**

The aim of the LCA was to estimate the global warming potential (GWP) of the CatMemReac technology being developed for micropollutant removal, particularly carbamazepine (CBZ). Two versions of the technology have been modeled and analyzed, namely the lab scale and the pilot scale. The LCA was conducted for both scales to identify the change in the GWP when the technology scale is upgraded. CBZ was the targeted pollutant, and it was reduced to below 1 ppb from the initial concentration of 1000 ppb, 20 ppb, and 5 ppb for both the lab as well as the pilot-scale setups.

The concentrations were chosen because it was scientifically convenient to measure 1000 ppb, and the limit of measurement was 20 ppb of CBZ. However, the available concentration of CBZ in natural water bodies, as well as wastewater treatment plant effluents, has been reported to be within 5 ppb (Cunningham et al., 2010<sup>26</sup>; Björlenius et al., 2018<sup>27</sup>). Therefore, the 5 ppb concentration was also analyzed to simulate the environmental impacts related to the practical concentration of the pollutant available in the environment.

The functional unit of the assessment was 1 m<sup>3</sup> of water treated by CatMemReac technology. The functional unit was the same for both scales. The system boundary included the operational phase input components such as pumps, nickel foam, electrophoretic deposition, and light-emitting diodes (LEDs), as shown in Figure 32. The input flows in the components were electricity and chemicals used in the operation of the lab and pilot scale setup components. The infrastructural components of the setup were not included as they were adopted on an availability basis in the lab. The infrastructure was not optimized and would also have a limited contribution to the environmental impacts, specifically the GWP of the product system (Rahman et al.<sup>28</sup>, 2018; Gallego-Schmid et al., 2019<sup>29</sup>).

The LCA was performed in the openLCA 2.0.0 software with the Ecoinvent database (ecoinvent 3.9.1) for the background data inventory required in the life cycle impact assessment.

### **2.1.2. Life Cycle Inventory Development**

The life cycle inventory was developed closely by working with the technical team at TAU. Most of the foreground operational data collected is primary in nature, directly from the technology developers. The background data inventory was adopted from the Ecoinvent

database, which is a widely adopted commercial database for LCA. The background data inventory for some components was not available and was developed using the literary sources in the openLCA software, but it was developed using literary sources in the openLCA software, as detailed below.

#### **2.1.2.1. Lab Scale Inventory Development**

The capacity of the lab scale setup was 100 ml per cycle. The electricity used in the pumping unit and EPD setup was calculated based on the rated capacity of the unit and operating hours collected from the technical team. The data about the amount of nickel foam used in the experimental setup was measured using a weighing balance. The background data inventory of nickel foam was not available; hence, the nickel foam process was developed using the data from the literature (Palmero et al., 2023<sup>30</sup>). The chemicals associated with the electrophoretic deposition (EPD) setup, such as solvents and catalyst, were collected from the technical team. The background data inventory for the zinc nitrate hexahydrate used in the EPD setup was not available. The process of zinc nitrate hexahydrate was developed using a patent that describes its preparation and provides the relevant amount of nitric acid and zinc oxide (August, 1965<sup>31</sup>; Costamagna et al., 2020<sup>32</sup>). The electricity associated with LED setup was estimated to be using the rated power of the setup at the desired wavelength provided by the manufacturer.

The technical team provided the time of operation for the concentration of CBZ analyzed along with the models. The model of 20 ppb CBZ degradation was adopted to calculate the time of operation for the degradation of 5 ppb CBZ through photocatalysis.

#### **2.1.2.2. Pilot Scale Experimental Setup**

The capacity of the pilot scale setup was 500 ml. The capacity enhancement was followed by a change in the size of nickel foam and components of setup such as pump, LED setup, sensors for electricity measurements and addition of chiller to maintain the temperature increased due to LED operations. The sensors gave the power used by the pump, LED, and chiller. However, the sensors were also one of the electricity consumers and provided real-time data with almost 12 data points in 10-second intervals. The weight of nickel foam was measured in the lab, while the technical team provided the resources used in the EPD setup and operation time for the setup. The background process of nickel foam developed for the lab-scale setup was utilized for the pilot-scale setup as well.

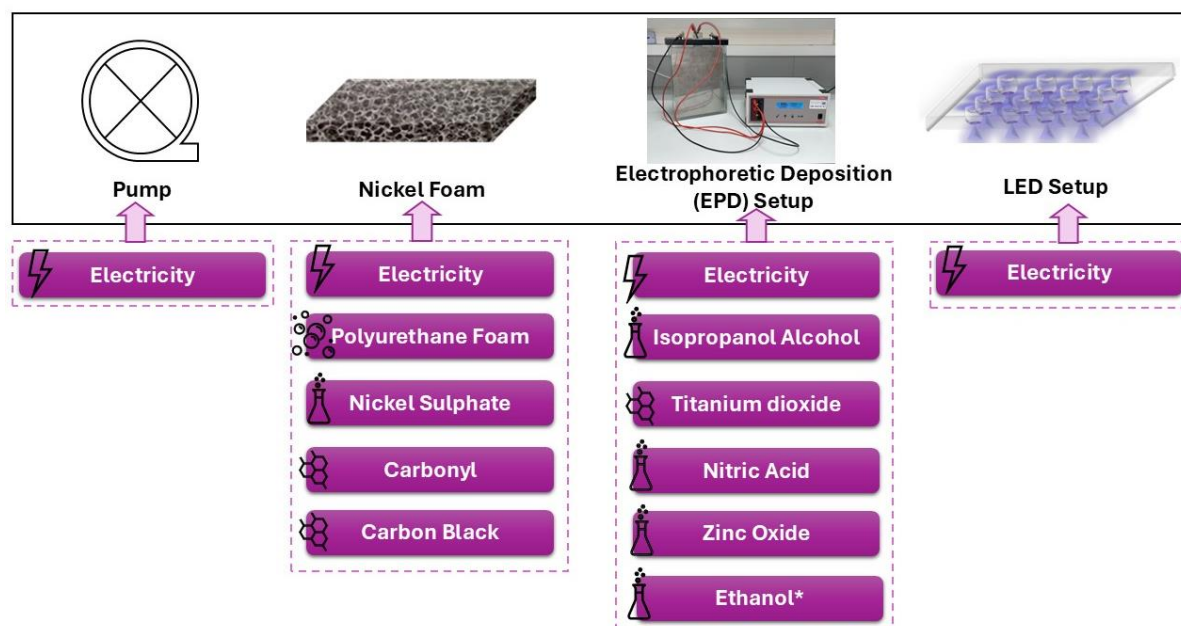


Figure 32: The system boundary showcasing the components of experimental setup and their input flows for both lab and pilot scale (\*only used in the lab scale EPD setup).

Table 8 summarizes the key developments in the pilot-scale setup compared to the lab-scale setup.

Table 8: The differences between different parameters in the lab and pilot scale setups.

Parameter	Lab Scale			Pilot Scale		
	5 ppb	20 ppb	1000 ppb	5 ppb	20 ppb	1000 ppb
Treatment Duration (minutes)	100.6	187.2	566.2	3.9	7.26	32.45
Treatment Volume (ml)		100			500	
Surface Area (cm <sup>2</sup> )		9.2			441	
Reaction Volume (cm <sup>3</sup> )		2.6			126	

### 2.1.3. Life Cycle Impact Assessment

The life cycle impacts were determined using the ReCiPe 2016 v1.03, a mid-point approach that uses IPCC models for global warming potential characterization factors. The ReCiPe method is widely adopted for determining the environmental impacts of emerging technologies in the domain of water treatment (Pesqueira et al., 2020<sup>33</sup>; Maniakova et al., 2023<sup>23</sup>). Thus, choosing the ReCiPe method also enables effective interpretation and

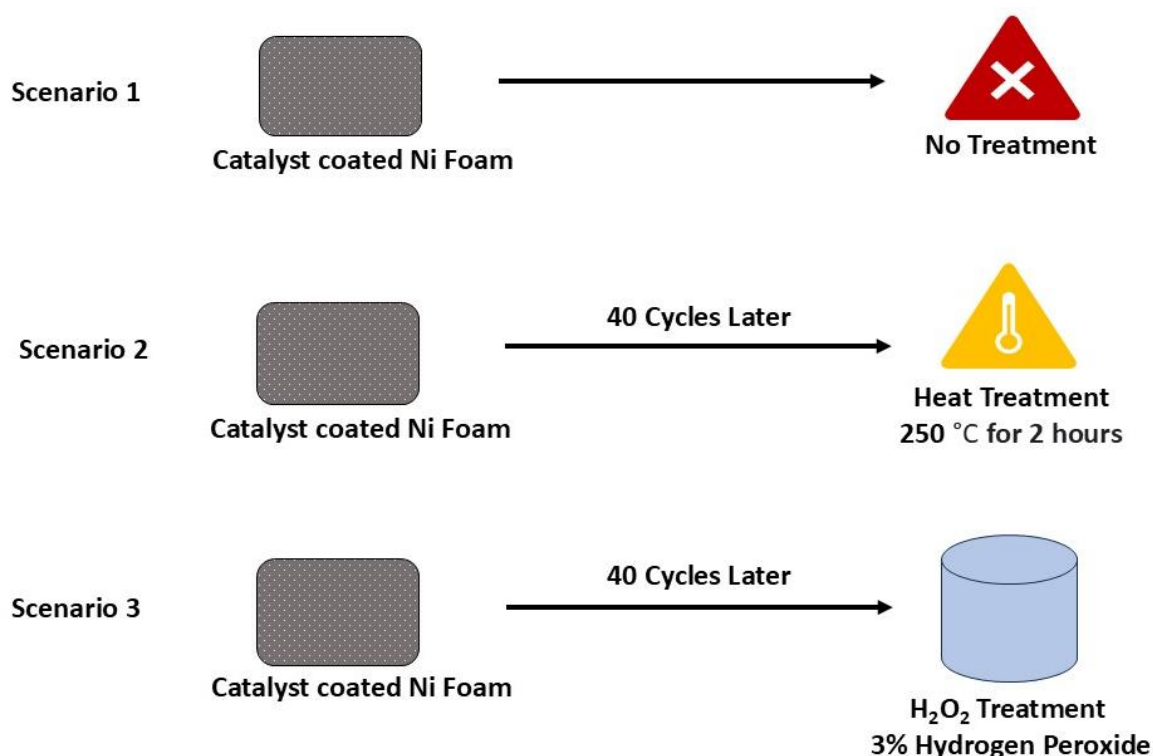
comparison of results for the CatMemReac technology with other competitive techniques. The ReCiPe 2016 method provides 17 environmental impact categories (Huijbregts et al., 2017<sup>34</sup>); however, due to the scope of the project, we focused on the global warming potential impacts of the lab as well as the pilot-scale setup.

#### **2.1.4. Uncertainty and Sensitivity Analysis**

The uncertainty and sensitivity assessments provide robustness to the outcomes of LCA. Due to the involvement of data from different sources, the uncertainty in the outcomes is part and parcel of LCA. Hence, it is imperative to estimate the uncertainty and provide the deviation in the mean global warming potential, which may occur due to variations in the input data inventory. The uncertainty associated with the foreground data inventory was investigated using a semi-quantitative approach given by Frischknecht et al.<sup>35</sup> (2005). This approach utilizes the pedigree matrix to provide data quality rating to the foreground inventory and determine the deviation in the data as shown in Equation 1. The values of the pedigree matrix and geometric standard deviation for each input flow are given in Table S3. The foreground data inventory is rated based on reliability ( $U_1$ ), completeness ( $U_2$ ), temporal correlation ( $U_3$ ), geographical correlation ( $U_4$ ), further technological correlation ( $U_5$ ), sample size ( $U_6$ ), and basic uncertainty factor ( $U_b$ ). The log-normal distribution was adopted, and Monte-Carlo simulations were performed with 10,000 iterations at a confidence interval of 90% in the openLCA software for both the lab as well as the pilot scale setups.

$$GSD^2 = \exp^{\sqrt{[\ln(U_1)]^2 + [\ln(U_2)]^2 + [\ln(U_3)]^2 + [\ln(U_4)]^2 + [\ln(U_5)]^2 + [\ln(U_6)]^2 + [\ln(U_b)]^2}} \quad (1)$$

The sensitivity assessment was performed to determine the differences in the methods associated with the reuse of nickel foam, resulting in its longevity and electricity grid mix used in the setup operations. During the treatment, the nickel foam may get attached to the biofilms, which may reduce its efficiency in pollutant removal. The technical team suggested treating the nickel using two techniques: heating for 2 hours at 250 °C or operating the reactor setup with 3% hydrogen peroxide ( $H_2O_2$ ), as shown in Figure 33.



*Figure 33: The scenarios for the treatment of nickel foam coated with titanium dioxide.*

The frequency of the nickel foam treatment was after 40 cycles as suggested by the experts in the technical team for both the lab and pilot scale setups. Global warming potential was also analyzed for the change in the electricity grid mix using the Ecoinvent database. For the analysis, the Israeli electricity mix was adopted. However the sensitivity analysis was conducted to see the variations in the GWP when the mix of Norway and China are used. This electricity grid mix represents the renewable intensive de-carbonized grid (Norway) and non-renewable intensive with high carbon intensity (China) sources in the electricity generation.

### **3. Results and discussion**

#### **3.1. Global Warming Potential Assessment**

The global warming potential (GWP) estimates for the lab and pilot scale setups operated at different CBZ concentrations are shown in Figure 34. The GWP of the lab-scale setup treating 1000 ppb of CBZ was the highest, followed by the other two concentrations. The difference between the lab and pilot-scale setup was significant, with 40 times less GWP in all the concentrations of CBZ analyzed. This difference in the GWP can be attributed to the time (minutes) of operation required for the desired treatment in the lab and pilot-scale setups.

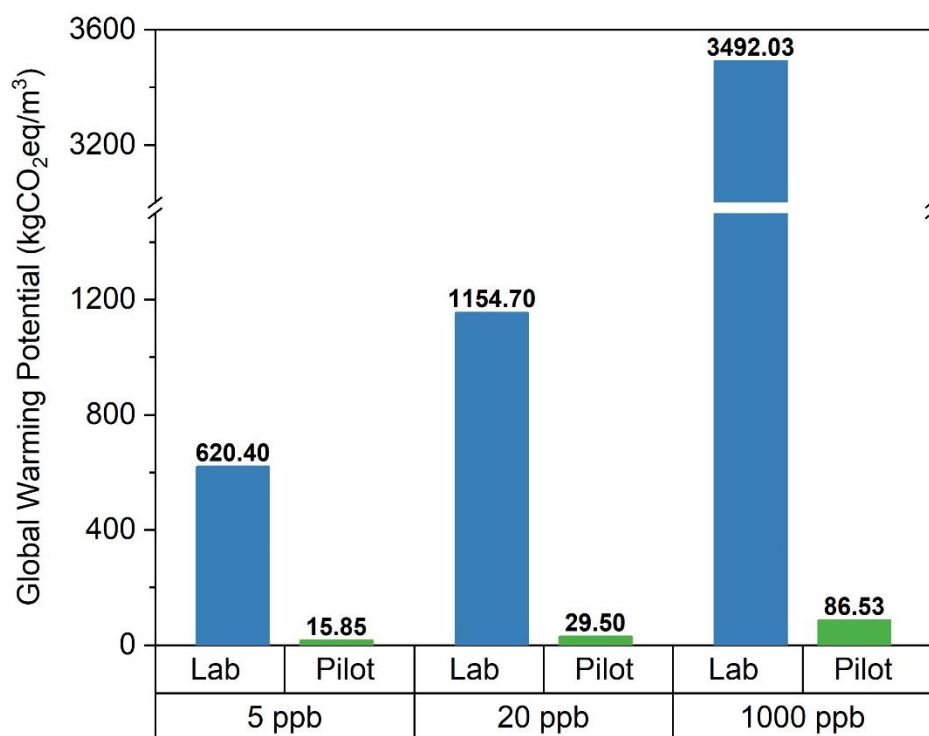


Figure 34: Global warming potential for the lab and pilot scale CatMemReac setup operated with different concentrations of carbamazepine.

As shown in Table 8, the time of operation for the pilot scale setup was relatively short in comparison to the lab scale setup for the degradation of CBZ. The time of operation in the pilot scale setup was reduced in accordance with the change in design parameters, including the surface area, as reported in Table 8. The surface area of the pilot scale setup was 48 times the lab scale setup. The lowest GWP was reported for the practical concentration of 5 ppb CBZ in the influent water sample treated in the pilot scale with a magnitude of 15.85 kgCO<sub>2</sub>eq for 1 cubic meter. Similarly, in CatMemReac technology, the major contributors to electricity use were the chiller, LEDs, pump, and sensors, contributing to 33%, 29%, 23%, and 15%, respectively (for 5 ppb CBZ treatment). The contribution of different input flows to the GWP in the lab and pilot scale setup is shown in Figure 35.

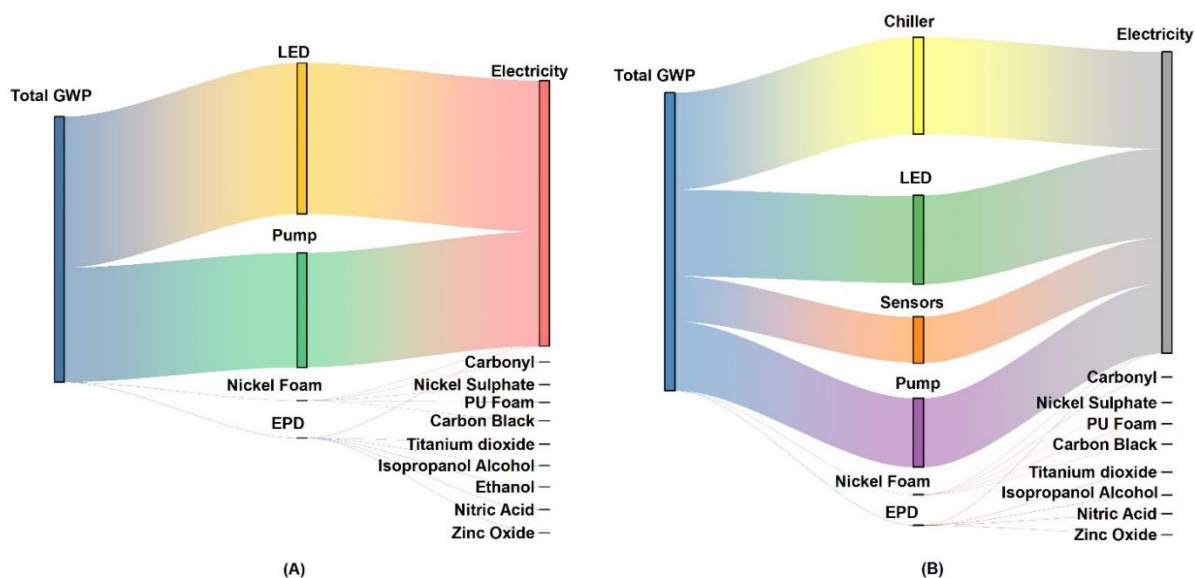


Figure 35: Contributions to global warming potential from different input flows in (A) Lab Scale and (B) Pilot Scale experimental setups.

The most contributing flow to the GWP in the lab as well as pilot scale setup was electricity use while the other consumables in nickel foam and EPD setup contribute insignificantly. The insignificant contribution to the total GWP is due to the lifetime of nickel foam and EPD setups. The nickel foam is a substrate on which the catalyst (titanium dioxide) is coated through the process of EPD.

The coated foam is relatively stable and is likely to operate for 15 years, as suggested by the experts. There is not much information available about the stability of nickel foam. However, it is reported that metallic foams are stable due to porous networks, which allows them an unlimited lifetime of operation capability in comparison to other common adsorbents (Zhang et al., 2024<sup>36</sup>). The nickel foam is prepared using polyurethane foam, which has an average lifetime of 15-20 years, which is another supportive evidence for the assumption to be considered conservative (Stergioudi et al., 2015<sup>37</sup>). The GWP is distributed throughout the entire lifetime of the component, and therefore, the nickel foam and EPD have lower contributions to the total emissions. The electricity use in lab scale setup is dominated by LED and pumping units, whereas in the lab scale setup, chiller and sensors are the additional units consuming energy. The chiller is required for cooling the LEDs. The requirement of the chiller is not in the lab scale setup as the LEDs are air-cooled by convection, so there is no electricity consumed. Similarly, during the development of the pilot scale, it was equipped with sensors to acquire real-time electricity use data. Nevertheless, the sensor is one of the major contributors to the electricity use in the pilot scale setup.



### 3.2. Uncertainty and Sensitivity Analysis

The data quality rating for the input flows is shown in Table 9. The values corresponding to electricity and chemicals used in the EPD setup are robust as they are the primary data adopted from the actual experimental conditions. The electricity of the lab scale in the pump and the LEDs of the pilot scale are less uncertain than the lab scale, as the former had sensors. The lab scale electricity determination adopts rated power and time of operation for the pump, LEDs, and EPD setup. The background inventory of nickel foam was adopted from literature as there was no proprietary process in the Ecoinvent database. The qualitative levels of uncertainty were mentioned in the literature which were used to generate quantitative ratings from the pedigree matrix. Similarly, the data for zinc oxide and nitric acid was also adopted from a patent, and therefore, the data ratings represent uncertainty.

*Table 9: The input flows with respective data quality ratings and geometric standard deviation.*

<i>Unit</i>	<i>Input Flow</i>	<i>Lab Scale</i>		<i>Pilot Scale</i>	
		<i>Data Quality<sup>\$</sup></i>	<i>GSD</i>	<i>Data Quality<sup>\$</sup></i>	<i>GSD</i>
<i>Pump</i>	<i>Electricity</i>	3,1,1,1,1,1,1.05	1.05	1,1,1,1,1,1,1.05	1.02
<i>LEDs</i>	<i>Electricity</i>	2,1,1,1,1,1,1.05	1.04	1,1,1,1,1,1,1.05	1.02
	<i>PU Foam</i>	4,5,1,3,1,1,1.05	1.14	4,5,1,3,1,1,1.05	1.14
<i>Nickel Foam</i>	<i>Nickel Sulphate</i>	3,3,1,3,1,1,1.05	1.06	3,3,1,3,1,1,1.05	1.06
	<i>Carbonyl</i>	3,3,1,3,1,1,1.05	1.06	3,3,1,3,1,1,1.05	1.06
	<i>Carbon Black</i>	4,5,1,4,1,1,1.05	1.14	4,5,1,4,1,1,1.05	1.14
	<i>Electricity</i>	3,3,1,3,1,1,1.05	1.06	3,3,1,3,1,1,1.05	1.06
	<i>Absolute Ethanol</i>	1,1,1,1,1,1,1.05	1.02	1,1,1,1,1,1,1.05	1.02
	<i>Isopropanol</i>	1,1,1,1,1,1,1.05	1.02	1,1,1,1,1,1,1.05	1.02
	<i>Alcohol</i>	1,1,1,1,1,1,1.05	1.02	1,1,1,1,1,1,1.05	1.02
<i>EPD Setup</i>	<i>Titanium dioxide</i>	1,1,1,1,1,1,1.05	1.02	1,1,1,1,1,1,1.05	1.02
	<i>Zinc Oxide</i>	2,1,2,3,1,1,1.05	1.04	2,1,2,3,1,1,1.05	1.04
	<i>Nitric Acid</i>	2,1,2,3,1,1,1.05	1.04	2,1,2,3,1,1,1.05	1.04
	<i>Electricity</i>	3,3,1,1,1,1,1.05	1.06	3,3,1,1,1,1,1.05	1.06
<i>Chiller</i>	<i>Electricity</i>	-	-	3,1,1,1,1,1,1.05	1.05
<i>Sensors</i>	<i>Electricity</i>	-	-	1,1,1,1,1,1,1.05	1.02

(\$ represents data quality rating corresponding to the reliability, completeness, temporal correlation, geographical correlation, further technological correlation and basic uncertainty

factor, respectively)

The component-specific and overall variation in the uncertainty of GWP resulting from the Monte Carlo simulation is shown in Table 10. The median value shows the simulation result, which is like the deterministic value from the LCA model, while the 5 and 95 percentiles show the lower and the upper bound variations. Results show that the lower and upper bound varies 6.8% and 7.2% from the mean value, respectively, in the lab scale setup. Similarly, the lower and upper bound of variation in the pilot scale were 5.4% and 5.6%, respectively. The uncertainty in the estimates of the pilot scale was low due to the use of sensors in the electricity consumption, which reduces the uncertainty in the estimation of GWP.

*Table 10: Uncertainty assessment showing the variations in the global warming potential values ( $\text{kgCO}_2\text{eq/m}^3$ ) for 5 ppb removal of CBZ.*

Components	Lab Scale Setup			Pilot Scale Setup		
	Median	5%	95%	Median	5%	95%
		Percentile	Percentile		Percentile	Percentile
<i>Pump</i>	267.58	244.79	291.91	3.67	3.52	3.82
<i>LEDs</i>	352.82	333.53	373.22	4.61	4.43	4.79
<i>EPD</i>	0.044	0.043	0.045	0.0032	0.0031	0.0034
<i>Nickel</i>	0.0068	0.0064	0.0072	0.0063	0.0059	0.0067
<i>Foam</i>						
<i>Sensors</i>	-	-	-	2.41	2.33	2.49
<i>Chiller</i>	-	-	-	5.15	4.71	5.62
<i>Total</i>	620.45	578.37	665.18	15.85	14.99	16.73

The sensitivity assessment results given in Figure 36 show the values of GWP when the nickel foam is treated with either  $\text{H}_2\text{O}_2$  or heat before being reused. The cleaning may be required with a certain water matrix, which can lead to the formation of biofilm, thus reducing the micropollutant degradation efficiency. The  $\text{H}_2\text{O}_2$  treatment is recommended as it enhances the longevity of nickel foam and has relatively low GWP compared to the heat treatment. In heat treatment, the use of a muffle furnace to keep the temperature in the range of 250 °C is energy-intensive, contributing to GHG emissions. Upon adoption of  $\text{H}_2\text{O}_2$  treatment, the GWP increases by 3% while the same is increased by 121% for the heat treatment in 5 ppb CBZ degradation at lab scale reactor setup. Similarly, the  $\text{H}_2\text{O}_2$  and heat treatment increases the GWP by 28% and 955%.

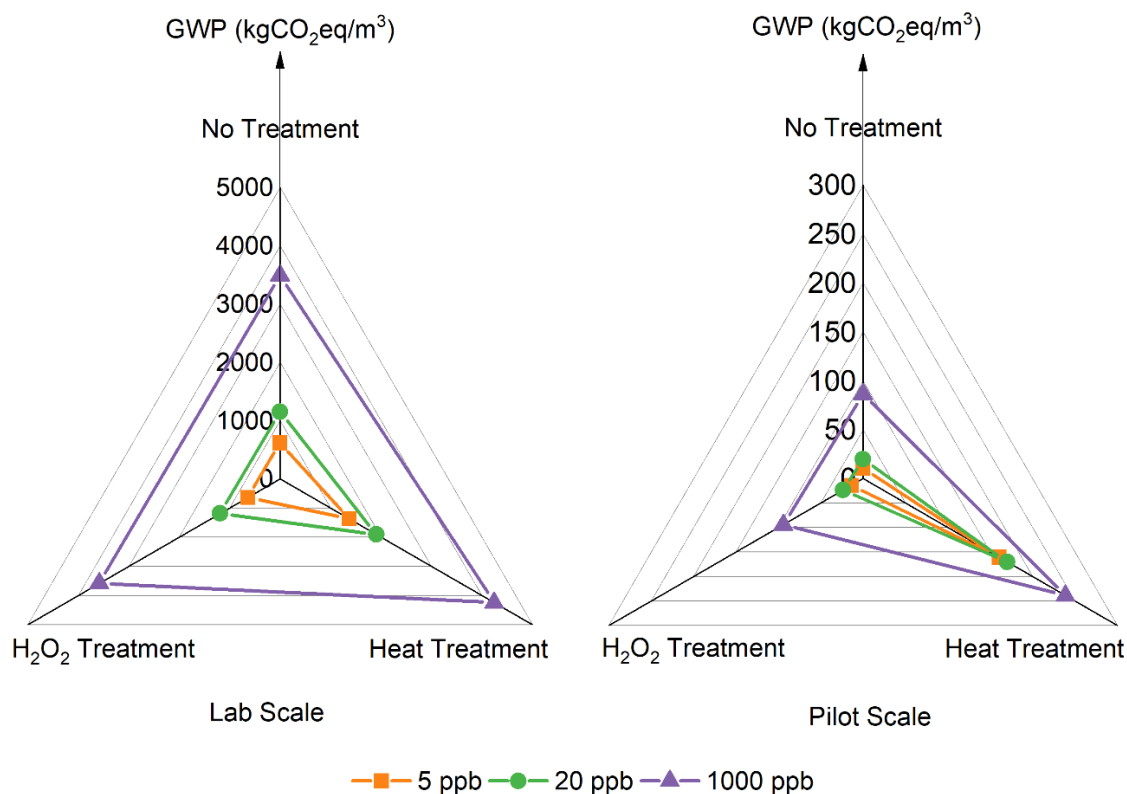


Figure 36: The variations in GWP for different treatment scenarios in associated with cleaning of nickel foam coated with catalyst.

The electricity grid mix is responsible for the characterization factor determining the global warming potential from a product system. Figure 37 shows the variations in the GWP for two different electricity grid mixes for the 5 ppb concentration of CBZ in lab and pilot scale setup. We choose the electricity grid of Norway and China with the characterization factor of 0.03 kgCO<sub>2</sub>eq/kWh and 1.49 kgCO<sub>2</sub>eq/kWh, respectively. Norway has a higher share of renewable energy sources, which results in lower GHG emissions per unit of electricity generation, while the China grid mix has a higher share of non-renewables. The Israeli grid mix was used primarily for the analysis and has a characterization factor of 0.79 kgCO<sub>2</sub>eq/kWh. The overall GWP was reduced by 96% in Norway, while it increased by 87% in China when operating the pilot scale setup. A similar trend was followed in the lab scale setup as well.

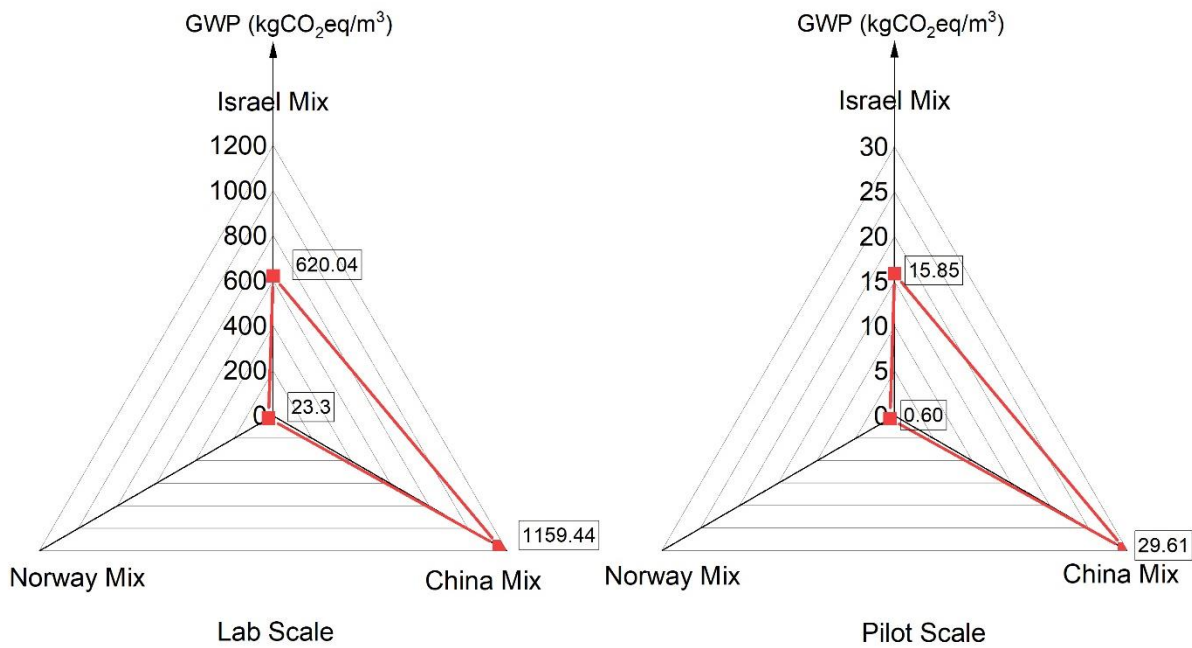


Figure 37: Variations in the GWP upon changing the electricity grid mix.

## **WP 8: Scenarios and global impact assessment**

### **4. Prospective LCA of CatMemReac technologies at TRL 9 (Led by Fraunhofer ISI)**

The task aimed to do a prospective life cycle assessment of an industrial-scale process of the CatMemReac technology based on the results for the lab and pilot scale. The SIMPL method (Langkau et al. 2023<sup>38</sup>) for prospective inventory modeling was applied. It involved several interviews and workshops with the technology developers of the CatMemReac team, as well as interviews with external experts. The results of the different steps will be described in the following sections.

#### **4.1. Goal and scope definition**

The prospective research question was formulated as follows:

*Will the CatMemReac technology have a lower global warming potential (GWP) than alternative technologies (ozonation, activated carbon) once it is market-ready (TRL 9) in 2030?*

The following scope definitions were agreed on through discussions within the entire CatMemReac project consortium and interviews with external experts:

- *Time horizon:* 2030 was chosen as time horizon, because it was estimated by the CatMemReac technology experts that the technology could reach TRL 9 by then, i.e. be in industrial application in 2030. Though external experts implied that it may take significantly longer to get this technology market ready, we kept the time horizon at

2030.

- *Scenario type:* We decided to develop an explorative best-case scenario for the CatMemReac technology to see if it is superior to conventional technologies regarding GHG emissions with optimistic assumptions on its further development. If GHG emissions are lower for the CatMemReac technology under best-case assumptions, alternative scenarios will be necessary to analyze which conditions must be given for the CatMemReac technology to have lower GHG emissions than conventional technologies. If GHG emissions of the CatMemReac technology are higher than GHG emissions of conventional technologies with these optimistic assumptions, this is an indication that the CatMemReac technology might not be able to reduce the GHG emissions of the removal of trace organic compounds.
- *Functional unit:* All calculations refer to the functional unit of 1 m<sup>3</sup> of treated wastewater fulfilling requirements of Swiss legislation, modelled by the reduction of 5 ppb CBZ by 80 %.
- *Application:* The standard application of an additional stage for existing large-scale wastewater treatment plants was assessed.
- *System boundaries:* Since the wastewater treatment plant will be the same for the conventional technologies and the CatMemReac technology, only the additional cleaning step was analyzed in the pLCA.
- *Geographical boundaries:* This pLCA investigated the environmental performance of the application of the CatMemReac technology in Germany as a likely application region, since removal of trace organic compounds is already applied in wastewater treatment plants in Germany and further application is motivated by the EU water directive.

#### **4.2. Inventory Analysis: Step A: Identify Relevant Parameters and Key Factors**

This step included:

- drawing a preliminary inventory model (step A1) to identify relevant inventory parameters,
- filling in a PESTEL checklist (step A2) to identify key factors outside the inventory model,
- drawing a causal loop diagram of the key factors and connecting them to the inventory parameters in the inventory model to show connections and relevance (step A3).

Two online workshops and several individual interviews within the project team helped to integrate the perspectives of the technology developers into these steps. Additionally, external

experts were asked to fill in the PESTEL checklist and review the results of the three steps. Preliminary sensitivity analysis with the preliminary inventory model identified the following inventory parameters as most relevant:

- electricity demand (for LEDs and pumping)
- electricity production (share of renewables)
- H<sub>2</sub>O<sub>2</sub> (or alternative chemicals) demand for cleaning
- H<sub>2</sub>O<sub>2</sub> production

Infrastructural components like the Ni-foam and its TiO<sub>2</sub> coating were found to have insignificant influence on the pLCA results due to their large lifetime (assumption: 15 years). Table 11 summarizes the results of the PESTEL analysis. The final Causal Loop Diagram connected to the inventory model is displayed in Figure 38. Finally, Table 12 gives an overview on the identified key factors and most relevant inventory parameters as the result of step A. In step B, assumption on these key factors and most relevant inventory parameters needed to be made.

*Table 11: Results of the PESTEL analysis (based on internal workshops and external expert consultation).*

Factors	Assessment
Political/Legal	<ul style="list-style-type: none"> <li>• Water policy <ul style="list-style-type: none"> <li>• legal requirements/recommendations for fourth cleaning step + removal targets for micropollutants (set by EU water directive à large scale implementation in Germany)</li> <li>• standards for operational safety of the treatment processes</li> </ul> </li> <li>• Climate policy <ul style="list-style-type: none"> <li>• targets for the share of renewables in the electricity mix</li> <li>• requirements for on-site electricity production at municipal wastewater treatment facilities</li> <li>• if policy/regulation sets targets for energy efficiency or energy consumption, it becomes a more relevant criterion for the selection of technologies for the fourth cleaning step</li> </ul> </li> </ul>

<b>Economic</b>	<ul style="list-style-type: none"> <li>Costs decide if and what technology is implemented for fourth cleaning step <ul style="list-style-type: none"> <li>mainly operation costs, also investment costs</li> <li>electricity costs play a key role for operation costs</li> <li>CO<sub>2</sub> prices could become relevant for the costs</li> </ul> </li> </ul>
<b>Social</b>	<ul style="list-style-type: none"> <li>Public perception of the fourth cleaning step: <ul style="list-style-type: none"> <li>is it seen as crucial for environmental protection or as a waste of money and resources due to the high energy consumption → depends on public awareness/anxiety of trace organic pollutants</li> <li>CatMemReac could be marketed as a ‚natural‘ photocatalytic process</li> </ul> </li> <li>Acceptance of water reuse <ul style="list-style-type: none"> <li>acceptance of water reuse for agriculture might grow in Germany due to increased drought issues</li> <li>fourth cleaning step can be seen as necessary for water reuse</li> </ul> </li> </ul>
<b>Technical</b>	<ul style="list-style-type: none"> <li>LEDs depend on critical raw materials → import dependency</li> <li>There is no market-ready TiO<sub>2</sub> catalyst available</li> <li>Technological progress of established technologies</li> </ul>
<b>Environmental</b>	<ul style="list-style-type: none"> <li>Relevance of the environmental problem of trace organic pollutants in comparison to other environmental problems (e.g. climate change, land use change)</li> <li>Relevance of the environmental problem of trace organic pollutants for other environmental problems (e.g. biodiversity loss)</li> </ul>



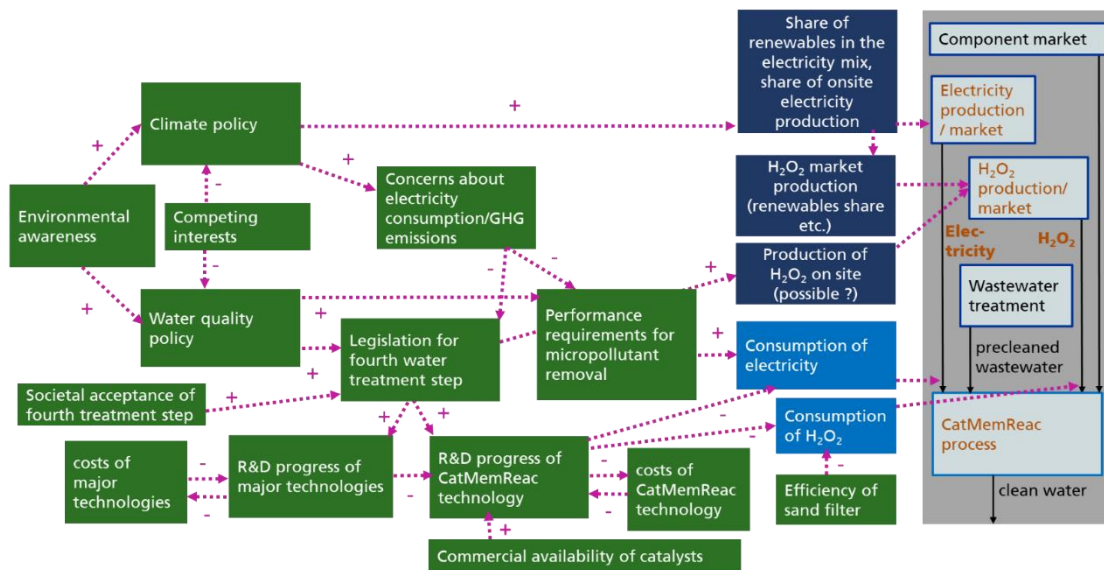


Figure 38: Causal loop diagram of key factors connected to the inventory parameters of the preliminary inventory model.

Table 12: Results of step A: Relevant inventory parameters and key factors.

#	Inventory parameters	Subordinate inventory parameters
I	Electricity demand	Electricity demand for LEDs, electricity demand for pumping
II	H <sub>2</sub> O <sub>2</sub> demand	Frequency of cleaning cycles, demand per cleaning cycle
III	Electricity production	Share or renewables in the energy mix, share of on-site production
IV	H <sub>2</sub> O <sub>2</sub> production	share of on-site production
#	Key factors	Influence on inventory parameters
v	Climate policy	III, IV (electricity mix), I, II (electricity scarcity → support of advanced treatment → techn. progr.)
vi	Water policy	I, II (technological progress), IV (technological progress)

#### 4.3. Inventory Analysis: Step B: Find future assumptions for each relevant inventory parameter and key factor

As part of the goal and scope phase, it was decided to develop an explorative best-case scenario for the CatMemReac technology to analyze if it has lower GHG emission than conventional technologies like ozonation with optimistic assumptions on its development. To make the respective best-case assumptions about each of the parameters and factors identified as relevant in step A, two interviews with external experts, as well as 8 interviews with technical experts of the CatMemReac consortium, were conducted.

Regarding the key factors and background parameters, it was assumed that Germany (as the defined geographical boundary, cf. goal and scope) will meet its announced climate policy

goals for 2030, resulting in a greener electricity mix than today. Furthermore, it was assumed that Germany will fulfill the EU water directive, which adopts Swiss requirements for the removal of trace organic compounds in a percentage of municipal wastewater treatment facilities by 2030. With more sophisticated assumptions on  $\text{H}_2\text{O}_2$  consumption for cleaning, it was found that the  $\text{H}_2\text{O}_2$  consumption does not influence the overall GHG emissions significantly, so no assumptions on alternative  $\text{H}_2\text{O}_2$  production on site were made. Since it was not possible to finish calculations of the CatMemReac technology and the conventional technologies for comparison with a German electricity mix of 2030, the comparison to conventional technologies will be made based on the German electricity mix at present. Since the electricity mix would change for all technologies, it is not expected that calculations with a future electricity mix will change the overall conclusions of this study.

Regarding foreground parameters, the following assumptions were made on improvements during further upscaling from the lab scale and pilot scale:

- *Reduction of the energy demand by optimization of the reactor geometry:* We assumed that the energy consumption for LEDs and pumping could be reduced by a factor of 150 starting from the lab-scale set-up through optimization of reactor geometry. This value is based on estimations of the CatMemReac technical team based on theoretical considerations and the experiences made in this project.
- *Reduction of the energy demand by optimization of the catalyst:* We assumed that an additional reduction of the electricity demand by 10% is possible by optimization of the catalyst, i.e. the usage of P25- $\text{TiO}_2$  with optimized crystal structures instead of the  $\text{TiO}_2$  used in the lab and pilot scale experiments.
- *Reduction of the energy demand by scaling effects of pumping:* we assumed that pumping efficiency would increase by 20 % from pilot scale to best-case industrial scale, because larger, more efficient and purpose-optimized pumps would be used in application scale.
- *Reduction of the energy demand by omitting sensors and cooling:* The pilot scale set-up had a significant energy demand for sensors, which are not necessary at industrial scale. Additionally, we assumed that cooling of LEDs will not be necessary because LEDs will be sufficiently cooled by the wastewater flow in the in the best-case industrial scale set-up.
- *Assumptions on reactor materials/infrastructural elements:* We neglected any potential changes regarding reactor materials/infrastructural elements since the lab/pilot scale analysis showed that they do not significantly influence the results of

the LCA. It is assumed that no replacement of infrastructural elements is necessary over the lifetime of the reactor.

- *Assumptions on reactor cleaning:* We assumed that sand filtering will remove cloudiness prior to CatMemReac treatment, so cleaning with H<sub>2</sub>O<sub>2</sub> once a month will be sufficient as is the case for other membrane applications.

These assumptions resulted in a GWP of 2.2 kg CO<sub>2</sub>eq/m<sup>3</sup> for the best-case industrial-scale scenario of the CatMemReac technology (Figure 39). It is driven by electricity use for LEDs and pumping while cleaning and infrastructural components together cause less than 0.1 % of these emissions. Due to the early stage of technological development and the many assumptions that needed to be made, this value has a high uncertainty. Further experiments under industrial conditions will be necessary for a more accurate estimate. Nonetheless, taking the optimistic character of the assumptions made and the fact that the resulting value is 8 times as high as the literature value for conventional technologies (0.28 kg CO<sub>2</sub>eq/m<sup>3</sup>), this is an indication that the CatMemReac technology might not be a promising option to reduce the GHG emissions of the removal of trace organic compounds in municipal wastewater treatment facilities. Besides the assumptions made, a further potential for reduction of GHG emissions of the CatMemReac technology would be using solar light instead of LEDs.

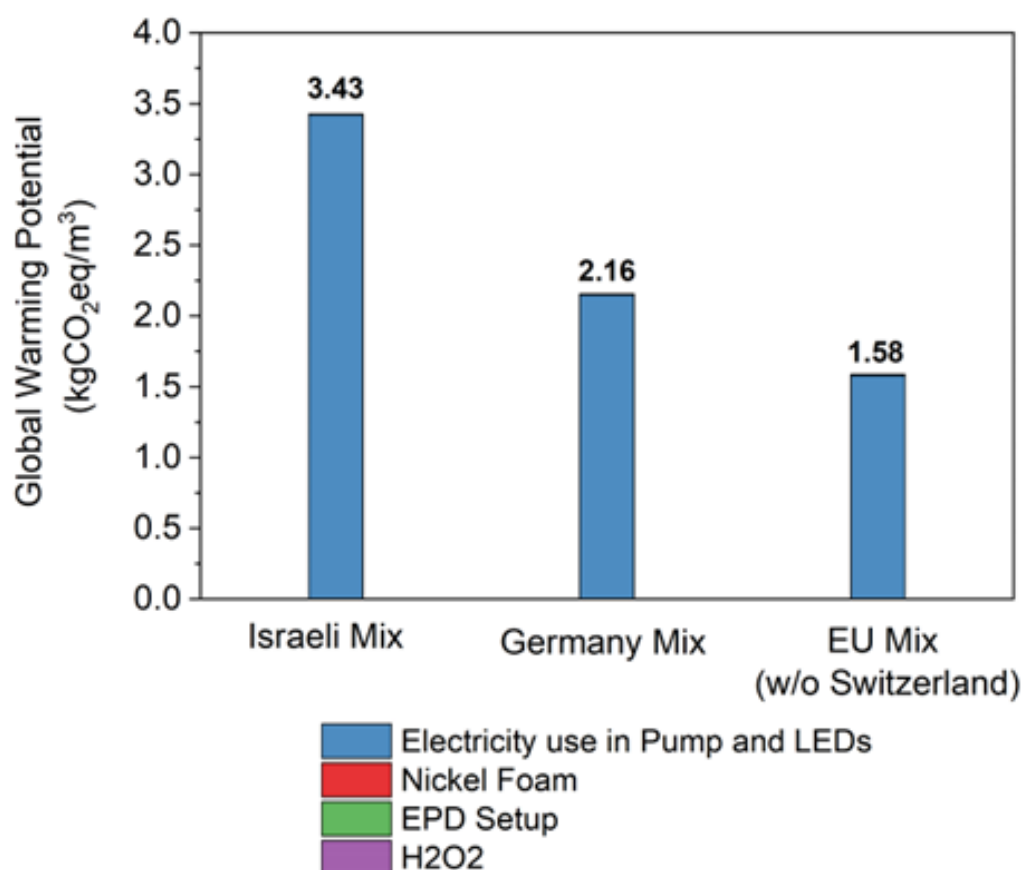


Figure 39: Global warming potential of a potential industrial-scale CatMemReac process according to a prospective LCA with optimistic assumptions for further technological development.

However, this would not be suitable for application in typical municipal wastewater treatment facilities, which are supposed to work independently of weather and daytime. The next chapter will discuss the potential applications of CatMemReac technology. Figure 39 compares the global warming potential of the prospective best-case industrial-scale CatMemReac process with the German, European, and Israeli electricity mix.

#### **4.4. Identification of application cases and potential impact-based (Led by TAU)**

The CatMemReac technology has shown the potential to reduce micropollutants, particularly CBZ. However, the sustainability assessment suggests that CatMemReac has higher GHG emissions compared to alternative technologies, such as ozone, at the moment and probably in the future scale. To assess the feasibility of CatMemReac, our approach was to map the wastewater treatment facilities in Israel and Germany to understand the level of treatment for possible reuse based on the location. However, due to the limitation of time and scanty amount of information available we decided to focus on Israel for assessing the feasibility of CatMemReac. We interviewed the officials working in water and wastewater treatment

systems to understand their perspectives on adopting advanced wastewater treatment in Israel. We got to know that one of the biggest wastewater treatment plants in Israel will be adopting Ozonation in the future as an alternative to soil aquifer treatment (SAT) for degrading micropollutants. As Israel reuses over 90% of its wastewater, the majority of which is used in agricultural fields, there have been problems associated with the bioaccumulation of micropollutants in irrigated crops. It has been reported that antibiotics in reclaimed wastewater being used for agriculture in Israel pose human health risks to the public utilization of the vegetables irrigated with wastewater (Mordechey et al., 2021). Therefore, it becomes imperative to analyze multiple advanced wastewater treatment solutions, which can be key for water-scarce regions around the world.

In our study, the best-case scenario with a prospective LCA approach estimates the value of GWP to be 2.16 kgCO<sub>2</sub>eq/m<sup>3</sup> compared to Ozone with the reported value of 0.3 kgCO<sub>2</sub>eq/m<sup>3</sup> (Tarpani and Azapagic, 2018). The GWP of CatMemReac is 86% higher than the Ozone treatment for reducing micropollutants. The higher value of GWP can be attributed to the electricity use in pumps and LEDs which makes the CatMemReac an energy intensive process. Nevertheless, the CatMemReac has an advantage of treating the micropollutant in a record time of less than 4 minutes for 5 ppb concentration (practical value in natural water matrix), which in case would take 20 to 30 minutes of contact time for the Ozone based treatment approach.

The feasibility of CatMemReac at a centralized wastewater treatment facility is doubtful due to the higher environmental impacts and availability of environmentally benign technology in the form of Ozone. Moreover, the Ozone based treatment approach saves the additional disinfection process. Although the CatMemReac can also contribute to the disinfection, its feasibility with different water matrices for simultaneous degradation of micropollutants and pathogens is a research gap for future studies.

Based on our discussion with Israeli officials involved in the planning of advanced wastewater treatment systems, the technology that can replace Ozonation must have the following advantages: economical and environmentally superior. The details of the interviewees are given in Table 13. Upon detailing the CatMemReac technology, the officials suggested that for now the technology can be a good option for the *decentralized* water treatment which could include groundwater or wastewater treatment for reuse. The assessment of CBZ removal in different water matrix in Figure 17 shows the potential of CatMemReac in groundwater while improvements in the form of pretreatment processes are needed for the actual wastewater treatment. This is because the Ozone in a decentralized setup can be costly

and has operational issues as it should be generated onsite. On the other hand, as per the experts' suggestions, superior removal of substances (emerging concerns) that are slow to react with, or inert to, ozone may become a strong reason to upscale and use CatMemReac technology in wastewater treatment plants (WWTP) in the future. We would be continuing research in the CatMemReac to look at how the technology develops and the reductions that could be achieved in carbon footprints and other relevant environmental impacts.

*Table 13: The details of the interviewees of the investigation to understand the feasibility of CatMemReac in Israel*

<i>Name of the Official</i>	<i>Position</i>	<i>Organization</i>	<i>Date of Interview</i>
<i>Shai Ezra</i>	Director of Water Quality Division	Mekorot	19th September, 2024
<i>Hadas Raanan Kiperwas</i>	Researcher and Policy Adviser, Environmental Health and Water Reuse	Mekorot	
<i>Shlomi Ben-Arush</i>	Chief Environmental Officer	IGUDAN	29th July, 2024

## **5. Conclusions**

The study presents the global warming potential (GWP) based on the life cycle assessment of the lab and pilot scale setup of CatMemReac technology for the degradation of carbamazepine (CBZ). The lab scale setup exhibits high global warming potential GWP due to the increased duration required for the degradation of CBZ. Improvement in the design, which includes an increase in the surface area of nickel foam being used as the substrate, reduces the reaction time from 100.6 minutes to 3.9 minutes for degrading 5 ppm CBZ in the lab and pilot scale setup, respectively. Therefore, the GWP for the lab scale setup was estimated to be 620.04 kgCO<sub>2</sub>eq/m<sup>3</sup>, while for the pilot scale, the value was 15.85 kgCO<sub>2</sub>eq/m<sup>3</sup>. The main contributor to the global warming potential was electricity use in pumps and LEDs in the lab, as well as pilot scale setup. Other consumables, such as solvents in electrophoretic deposition and nickel foam, had 15 years of service life, leading to an insignificant share in the GWP for both lab and pilot-scale setups. The use of primary data acquired from the technical team in most of the input flows limits the uncertainty in the assessment. The sensitivity analysis shows 96% reduction in GWP for the greener electricity grid mix compared to the Israeli mix for the CatMemReac. The magnitude of the value for the greener mix is 0.6 kgCO<sub>2</sub>eq/m<sup>3</sup>, which is

twice as reported for Ozone treatment and has the potential to be reduced with further development in the CatMemReac technology. Although the CatMemReac technology is energy and emission-intensive compared to the Ozone treatment, the technology shows the potential to be applied for decentralized treatment of groundwater and wastewater where Ozone may face operational issues.

### **List of Publications**

#### ***Submitted (Waiting for response)***

1. Carbamazepine Degradation with TiO<sub>2</sub> EPD-coated over 3D Nickel Foam in a Photocatalytic Flow Reactor

#### ***To be Submitted***

1. Life Cycle Assessment of CatMemReac: Evaluating Impact Reduction Potential in the Transition from Lab to Pilot Scale Setup.
2. Prospective Life Cycle Assessment of Industrial Scale CatMemReac Technology: Feasibility and Comparative Assessment.
3. Carbamazepine Degradation Upscaled Photocatalytic Flow Reactor Based EPD-Coated TiO<sub>2</sub> Over 3D Ni Foam

### **References**

1. Horovitz, I. *et al.* Carbamazepine degradation using a N-doped TiO<sub>2</sub> coated photocatalytic membrane reactor: Influence of physical parameters. *J Hazard Mater* **310**, 98–107 (2016).
2. Liu, C. F., Huang, C. P., Hu, C. C., Juang, Y. & Huang, C. Photoelectrochemical degradation of dye wastewater on TiO<sub>2</sub>-coated titanium electrode prepared by electrophoretic deposition. *Sep Purif Technol* **165**, 145–153 (2016).
3. Wang, M. *et al.* Repeated photocatalytic inactivation of E. coli by UV + Ni foam@TiO<sub>2</sub>: Performance and photocatalyst deactivation. *Chemical Engineering Journal* **468**, (2023).
4. C Hamaker, B. H. *FORMATION O F A DEPOSIT BY ELECTRO-PHORESIS.*
5. Obregón, S., Amor, G. & Vázquez, A. Electrophoretic deposition of photocatalytic materials. **269**, 236–255 (2019).
6. Radice, S., Bradbury, C. R., Michler, J. & Mischler, S. Critical particle concentration in electrophoretic deposition. *J Eur Ceram Soc* **30**, 1079–1088 (2010).

7. Wang, Y. Q., Byun, J. H., Kim, B. S., Song, J. Il & Chou, T. W. The use of Taguchi optimization in determining optimum electrophoretic conditions for the deposition of carbon nanofiber on carbon fibers for use in carbon/epoxy composites. *Carbon N Y* **50**, 2853–2859 (2012).
8. Halanur Mruthunjayappa, M., Shachar, C., Imbar, A., Menashe, O. A. & Mamane, H. Cellulose acetate and polycaprolactone based photoactive ultrafiltration membrane: A novel approach with UV-switchable photocatalytic activity. *Sep Purif Technol* **329**, (2024).
9. Zhu, Y. C. *et al.* Three-Dimensional TiO<sub>2</sub>@Cu<sub>2</sub>O@Nickel Foam Electrodes: Design, Characterization, and Validation of O<sub>2</sub>-Independent Photocathodic Enzymatic Bioanalysis. *ACS Appl Mater Interfaces* **11**, 25702–25707 (2019).
10. V, V. K., Avisar, D., V, L. P., Betzalel, Y. & Mamane, H. Rapid visible-light degradation of EE2 and its estrogenicity in hospital wastewater by crystalline promoted g-C<sub>3</sub>N<sub>4</sub>. *J Hazard Mater* **398**, 122880 (2020).
11. Kanakaraju, D., Glass, B. D. & Oelgemöller, M. Advanced oxidation process-mediated removal of pharmaceuticals from water: A review. *J Environ Manage* **219**, 189–207 (2018).
12. Lee, S. Y. & Park, S. J. TiO<sub>2</sub> photocatalyst for water treatment applications. *Journal of Industrial and Engineering Chemistry* **19**, 1761–1769 (2013).
13. Fernández, P., Blanco, J., Sichel, C. & Malato, S. Water disinfection by solar photocatalysis using compound parabolic collectors. *Catal Today* **101**, 345–352 (2005).
14. Ong, C. S. *et al.* The impacts of various operating conditions on submerged membrane photocatalytic reactors (SMPR) for organic pollutant separation and degradation: A review. *RSC Adv* **5**, 97335–97348 (2015).
15. Selvam, K., Muruganandham, M., Muthuvel, I. & Swaminathan, M. The influence of inorganic oxidants and metal ions on semiconductor sensitized photodegradation of 4-fluorophenol. *Chemical Engineering Journal* **128**, 51–57 (2007).
16. Bhatkhande, D. S., Pangarkar, V. G. & Beenackers, A. A. C. M. Photocatalytic degradation for environmental applications - A review. *Journal of Chemical Technology and Biotechnology* vol. 77 102–116 Preprint at <https://doi.org/10.1002/jctb.532> (2002).
17. Huang, J. & Mabury, S. A. A new method for measuring carbonate radical reactivity toward pesticides. *Environ Toxicol Chem* **19**, 1501–1507 (2000).



18. Kim, M. J., Choo, K. H. & Park, H. S. Photocatalytic degradation of seawater organic matter using a submerged membrane reactor. *J Photochem Photobiol A Chem* **216**, 215–220 (2010).
19. Risch, E., Jaumaux, L., Maesele, C. & Choubert, J. M. Comparative Life Cycle Assessment of two advanced treatment steps for wastewater micropollutants: How to determine whole-system environmental benefits? *Science of the Total Environment* **805**, (2022).
20. Mousel, D., Palmowski, L. & Pinnekamp, J. Energy demand for elimination of organic micropollutants in municipal wastewater treatment plants. *Science of the Total Environment* **575**, 1139–1149 (2017).
21. Meier, A. *et al.* Die Behandlung Des Kommunalen Abwassers Mit Ozon Oder Aktivkohle Verringert Den Eintrag an Organischen Spurenstoffen in Die Gewässer. Aufgrund Der Notwendigen Betriebsmittel Werden Dabei Die Treibhausgasemissionen Erhöht. Der Vorliegende Artikel Zeigt Auf, Welche Massnahmen ARA-Betreiber Ergreifen Können, Um Diesen Anstieg Des CO<sub>2</sub>-Fussabdrucks Zu Minimieren. Vielfach Können Mit Diesen Massnahmen Auch Die Betriebskosten Gesenkt Werden.
22. de Boer, S., González-Rodríguez, J., Conde, J. J. & Moreira, M. T. Benchmarking tertiary water treatments for the removal of micropollutants and pathogens based on operational and sustainability criteria. *Journal of Water Process Engineering* vol. 46 Preprint at <https://doi.org/10.1016/j.jwpe.2022.102587> (2022).
23. Maniakova, G., Polo López, M. I., Oller, I., Malato, S. & Rizzo, L. Ozonation Vs sequential solar driven processes as simultaneous tertiary and quaternary treatments of urban wastewater: A life cycle assessment comparison. *J Clean Prod* **413**, (2023).
24. Arzate, S., Pfister, S., Oberschelp, C. & Sánchez-Pérez, J. A. Environmental impacts of an advanced oxidation process as tertiary treatment in a wastewater treatment plant. *Science of the Total Environment* **694**, (2019).
25. Muñoz, I., Rodríguez, A., Rosal, R. & Fernández-Alba, A. R. Life Cycle Assessment of urban wastewater reuse with ozonation as tertiary treatment. A focus on toxicity-related impacts. *Science of the Total Environment* **407**, 1245–1256 (2009).
26. Cunningham, V. L., Perino, C., D'Aco, V. J., Hartmann, A. & Bechter, R. Human health risk assessment of carbamazepine in surface waters of North America and Europe. *Regulatory Toxicology and Pharmacology* **56**, 343–351 (2010).
27. Björlenius, B. *et al.* Pharmaceutical residues are widespread in Baltic Sea coastal and offshore waters – Screening for pharmaceuticals and modelling of environmental

- concentrations of carbamazepine. *Science of the Total Environment* **633**, 1496–1509 (2018).
28. Rahman, S. M., Eckelman, M. J., Onnis-Hayden, A. & Gu, A. Z. Comparative Life Cycle Assessment of Advanced Wastewater Treatment Processes for Removal of Chemicals of Emerging Concern. *Environ Sci Technol* **52**, 11346–11358 (2018).
  29. Gallego-Schmid, A. *et al.* Environmental assessment of solar photo-Fenton processes in combination with nanofiltration for the removal of micro-contaminants from real wastewaters. *Science of the Total Environment* **650**, 2210–2220 (2019).
  30. Palmero P.J., Kärnman, T., Martínez-Pardo, P., Nilsson, C., Holmquist, H., Johansson, MJ. *et al.* Electrochemical Reduction of Alkenes over a Nickel Foam Guided by Life Cycle, Safety and Toxicological Assessments. ChemRxiv. (2023); doi:10.26434/chemrxiv-2023-p4q71
  31. August, M. Process for Preparing Pulverulent Hydrates of Zinc Nitrate. Patent US3206281A (1965). *United States Patent Office*.
  32. Costamagna, M., Ciacci, L., Paganini, M. C., Calza, P. & Passarini, F. Combining the highest degradation efficiency with the lowest environmental impact in zinc oxide based photocatalytic systems. *J Clean Prod* **252**, (2020).
  33. Pesqueira, J. F. J. R., Pereira, M. F. R. & Silva, A. M. T. Environmental impact assessment of advanced urban wastewater treatment technologies for the removal of priority substances and contaminants of emerging concern: A review. *Journal of Cleaner Production* vol. 261 Preprint at <https://doi.org/10.1016/j.jclepro.2020.121078> (2020).
  34. Huijbregts, M. A. J. *et al.* ReCiPe2016: a harmonised life cycle impact assessment method at midpoint and endpoint level. *International Journal of Life Cycle Assessment* **22**, 138–147 (2017).
  35. Frischknecht, R. *et al.* The ecoinvent database: Overview and methodological framework. *International Journal of Life Cycle Assessment* vol. 10 3–9 Preprint at <https://doi.org/10.1065/lca2004.10.181.1> (2005).
  36. Zhang, Z. *et al.* “Floating Catalytic Foam” with prominent heat-induced convection for the effective photocatalytic removal of antibiotics. *J Hazard Mater* **463**, (2024).
  37. Stergioudi, F. *et al.* Copper foams in water treatment technology: Removal of hexavalent chromium. *Mater Des* **87**, 287–294 (2015).

38. Langkau, S. *et al.* A stepwise approach for Scenario-based Inventory Modelling for Prospective LCA (SIMPL). *International Journal of Life Cycle Assessment* **28**, 1169–1193 (2023).